Control of flagellum length by a grow-and-lock model

Eloïse Bertiaux[1,2,4], Benjamin Morga[1,3,4], Thierry Blisnick[1], Brice Rotureau[1] & Philippe Bastin[1,5]

[1]Trypanosome Cell Biology Unit, Institut Pasteur & INSERM U1201, 25, rue du Docteur Roux, 75015 Paris, France.

[2]Université Pierre et Marie Curie Paris 6, Cellule Pasteur-UPMC, 25 rue du Docteur Roux, 75015 Paris, France

[3] Present address: Laboratoire de Génétique et Pathologie des Mollusques Marins, Station de La Tremblade - Ronce Les Bains - 17390 La Tremblade, France

[4] Equal contribution

[5] Lead contact: pbastin@pasteur.fr

SUMMARY

Several cell types such as photoreceptors and spermatozoa possess very stable cilia and flagella, a feature also encountered in numerous protists. We tested an original model for the control of flagellum length in such cells, using *Trypanosoma brucei* as an experimental system. The grow-and-lock model proposes that the flagellum elongates at a linear rate and that a locking event takes place in a timely defined manner preventing further elongation or shortening. We show that the total amount of IFT material increases during flagellum elongation, ensuring a constant concentration per unit of length and the ability to provide a constant delivery of precursors in agreement with a linear growth rate. Reducing the IFT rate by RNAi knockdown of the IFT kinesin motors slows down the growth rate and results in the assembly of shorter flagella. The flagellum is locked after cell division in an irreversible process and even subsequent increase in the IFT rate does not lead to further elongation. Other models (limitation by the soluble pool of tubulin, equilibrium between assembly and disassembly rates, or morphogenetic control) fail to explain the experimental data. The locking event is associated to the addition of the FLAM8 molecular marker at the distal end of the flagellum and is initiated prior cell division, leading to an arrest of elongation in the daughter cell. These results provide support for the grow-and-lock model as a new paradigm for the control of organelle length.

Keywords: cilia and flagella; ciliogenesis; organelle length; microtubules; intraflagellar transport; trypanosome; photoreceptor; spermatozoa

INTRODUCTION

Cilia and flagella (interchangeable terms) are present at the surface of many eukaryotic cells from protists to humans where they are involved in a range of functions including motility, sensing or morphogenesis. Multiple types of ciliary organisations are encountered from one species to another, and also between different cells in the same organism. Striking variations have been noted in cilia composition, positioning or length, presumably reflecting an optimisation related to the function in a given cell type. The lifespan of cilia is also highly variable, from the transitory existence of some primary cilia to the very stable cilia or flagella of photoreceptors or spermatozoa that show little or no turnover of their microtubules.

Despite extensive variation, each cilium or flagellum exhibits a defined length, a process that has fascinated scientists for decades [1]. To decipher the mechanisms that control length, it is essential to understand how the organelle is constructed. Tubulin is delivered via Intraflagellar Transport (IFT) to the distal end of growing microtubules where incorporation takes place [2-4]. Absence of IFT prevents cilium construction in all organisms investigated so far [5]. The control of flagellum length has mostly been studied in the green algae *Chlamydomonas* [6], a member of the Archeoplastida group [7]. In this organism, flagellar microtubules are highly dynamic and exhibit constant disassembly at their plus end. In such a situation, IFT is essential not only for the construction but also for the maintenance of length [8]. Several models have been proposed to explain the control of length in this context, mainly as a balance between assembly and disassembly rates [6], with IFT being a central component [4, 8-11]. These models could function in other systems where cilia display significant microtubule turnover such as in *C. elegans* [12] but could not be applied in cells with more stable cilia.

In mammals, the mouse sperm flagellum relies on IFT for assembly but not for maintenance, and yet the sperm flagellum does not disassemble after maturation [13]. Another case is the connecting cilium of photoreceptors in the retina. These cells display very low turnover [14] and loss of IFT after assembly only impacts ciliary length after 2-3 weeks, possibly because the cell degenerates [15]. How is length control achieved in such conditions? Here, we propose a new model termed grow-and-lock where the organelle grows up to a stage where a signal blocks further elongation or shortening by inducing a modification that locks the structure in a stable (or mature) configuration. The organelle is now ready to perform its final function and does not need length monitoring. In theory, this model is compatible with any type of assembly rate but the easiest situation is to assume a linear growth rate. The moment when the flagellum is locked could be controlled at the level of the flagellum itself, thereby implying a way to measure length. A simpler option would be to link that event to another cellular process that is timely regulated, such as progression through the cell cycle or through cell differentiation. The locking event would lead to a modification of the organelle that makes its structural elements very stable whereas other components could remain dynamic. Alternatively, it could prevent access of tubulin dimers and other components to the flagellum. This simple model predicts that cells could produce flagella of different lengths by modulating the growth rate and/or the timing of the locking event.

Spermatozoa or photoreceptors do not lend easily to manipulation. By contrast, protists represent great model organisms, are amenable in the laboratory and several of them exhibit very stable flagella. Here, we selected the protist *Trypanosoma brucei* for the investigation of the grow-and-lock model for several reasons. First, its axoneme is very stable [16] and relies on IFT for construction [17, 18] but not for length maintenance [19], exactly like in spermatozoa or photoreceptors. IFT remains active after assembly to maintain other elements but not axoneme composition [19]. Second, when trypanosomes infect mammals or

tsetse flies, they progress through several stages of development during which they assemble flagella of different length [20-22] and composition [23]. This is reminiscent to what multi-cellular organisms do in different cell types and means that the system is flexible. Third, trypanosomes grow well in culture; they assemble their flagellum in a timely, reproducible and well-characterised manner [24-26]; they are amenable to reverse genetics and IFT has been exhaustively quantified [27].

In this study, we provide experimental evidence that supports each of the major predictions of the grow-and-lock model. We show that results are not compatible with three other possible models: limited pool of soluble tubulin, equilibrium between assembly and disassembly and control by cell body length. The growth rate of the trypanosome flagellar is linear thanks to the continuous recruitment of new IFT trains in the elongating flagellum and its reduction upon IFT kinesin knockdown results in the construction of shorter flagella. The locking event is controlled at the cell cycle level, is triggered prior cell division and is correlated to the addition of a unique marker protein. The fact that the flagellum is locked is supported by the fact that increasing the IFT rate after maturation does not result in further elongation. Blocking cell division allows for the construction of longer flagella that ultimately mature and reach exactly the same length as the flagellum assembled in the previous generation. The grow-and-lock model provides an opportunity to explain the control of flagellum length in cells with very stable organelles.

RESULTS

IFT delivery remains constant during flagellum construction

The simplest version of the grow-and-lock model is based on a linear growth rate. This is exactly the case of flagellum assembly in *T. brucei* as measured in culture [25] and during animal infection [28]. This implies a constant delivery of tubulin by IFT no matter the stage of elongation. So far, IFT has only been quantified in mature flagella of *T. brucei* at the procyclic stage maintained in culture [27, 29]. Here, IFT trafficking was examined in the elongating flagellum and compared to the mature flagellum that remains present during the cell cycle, providing an ideal control [24]. This was carried out in live procyclic trypanosomes that express a fusion protein between the fluorescent Tandem Tomato protein (TdT)[30] and the IFT-B protein IFT81, upon endogenous tagging in the *IFT81* locus [31]. In addition to the bright signal at the base, a succession of motile spots was detected all along the length of the flagellum moving in either anterograde or retrograde direction in cells with a single flagellum (Video 1, Fig. 1A1) or in those assembling the new one, hence possessing two flagella (Videos 2-4, Fig. 1 A2-4). A summary of flagellum elongation during the trypanosome cell cycle is presented at Figure S1A. At first glance, IFT behaviour looked quite similar in both growing and mature flagella (Fig. 1A). The total amount of fluorescence emitted by the TdT::IFT81 protein in the flagellar compartment was quantified by using the first image of each movie. Plotting the ratio between the total amount of fluorescence in the new flagellum and that in the old one versus the length of the growing flagellum demonstrated a linear correlation between these two parameters (Fig. 1C). This data shows that IFT proteins are progressively recruited to the flagellum as it elongates. This means that the IFT amount increases linearly with length hence IFT density per unit of length of length remains constant during elongation.

Next, kymograph analysis [27] was carried out to quantify IFT rates and frequencies in cells with one (Fig. 1A1 and Fig. 1B1) or two flagella at different steps of elongation (Fig. 1A2-4 and Fig 1B2-4). Kymograph observations revealed brighter individual tracks for anterograde transport and less intense tracks for retrograde transport as expected [27]. Both IFT speed (Fig. 1D) and frequency (Fig. 1E) were invariant during flagellum elongation (Table 1), supporting a constant delivery rate of material at the tip of the growing flagellum. We conclude that the IFT delivery rate remains constant during flagellum construction, which is in agreement with the reported linear growth rate [25, 28].

Knockdown of IFT kinesins reduces frequency and speed of IFT and results in the assembly of short flagella

The grow-and-lock model implies that modulation of the flagellum growth rate would impact on the final length reached by the organelle. To reduce IFT trafficking, we selected to deplete the expression of kinesin II, the IFT anterograde motor. The genome of *T. brucei* encodes two putative kinesin II proteins (Tb927.5.2090 and Tb927.11.13920) but no kinesin-associated protein (KAP) [32, 33]. Individual RNAi silencing of KIN2A or KIN2B did not result in a visible phenotype: cells assembled apparently normal flagella and grew normally in culture (data not shown), suggesting redundancy. Hence simultaneous knockdown of KIN2A and KIN2B was performed following stable transformation of trypanosomes with a plasmid expressing dsRNA of both *KIN2A* and *KIN2B* under the control of tetracycline-inducible promoters [34]. The efficiency of RNAi silencing in $KIN2A2B^{RNAi}$ cells was confirmed by western blotting using an antibody against KIN2B [33](Fig. S2). The signal for KIN2B dropped by at least 8-fold from day 1 and remained low for at least 6 days, confirming the efficiency of RNAi silencing (Fig. S2). The frequency and speed of IFT was examined upon transformation of $KIN2A2B^{RNAi}$ cells with the reporter construct described above allowing

endogenous tagging of IFT81 with TdTomato. Trypanosomes were grown in induced or non-induced conditions and IFT was measured in live uniflagellated cells upon kymograph analysis. In control cells, bright anterograde trains were frequently observed, trafficking from the base to the tip of the flagellum where they were transformed to retrograde trains (Fig. S3A & Video 5). Kymograph analysis revealed that the average anterograde speed was 1.7±0.5 $\mu m.s^{-1}$ (n=159 trains from 10 separate cells) and the mean frequency was 0.64 $train.s^{-1}$ (Fig. S3B & Table 2). RNAi-induced cells looked different, the signal at the base of the flagellum appeared brighter and adopted a more elongated shape compared to that in control cells (Fig. S3C). The train frequency was reduced to $0.37.s^{-1}$ (n=95) after one day of induction, and down to $0.25.s^{-1}$ after 4 to 6 days in RNAi conditions (n=125)(Video 6)(Table 2). This is visible on the kymograph with fewer traces in induced cells (Fig. S3D) compared to control ones (Fig. S3B). In addition, IFT trains travelled more slowly when kinesin expression was knocked down: 1.4 $\mu m.s^{-1}$ at days 4 or 6 instead of 1.9 $\mu m.s^{-1}$ at day 0 (Fig. S3D)(Table 2). We conclude that the joint depletion of KIN2A and KIN2B expression efficiently reduced IFT delivery in the flagellum.

The observed 3-fold reduction in IFT train frequency should result in a significant reduction in the flagellum growth rate that should consequently allow testing the impact of this parameter on the grow-and-lock model. Monitoring the culture by microscopy during the course of RNAi indicated the presence of smaller cells with a shorter flagellum (Fig. 2A). To quantify this reduction, cells were fixed, processed for immunofluorescence assay (IFA) using the axonemal marker Mab25 and DAPI for DNA staining, and the length of the flagellum was measured. Cells that possessed a single flagellum were first examined. In non-induced samples, the length of the axoneme was on average ~20 µm, as expected [24]. However, the length of the flagellum was shorter during the course of RNAi induction, down to ~9 µm at

day 4. Despite the large dispersion, this difference was statistically significant (Fig. 2B). Flagellum length remained in that range over the next two days of induction (Fig. 2B), and up to 11 days after having triggered kinesin knockdown (not shown). In control non-induced samples, analysis by scanning electron microscopy revealed the typical elongated trypanosome shape with the flagellum attached to the cell body (Fig. 2C). By contrast, flagellum length was clearly shorter in induced cells that displayed a shorter cell body (Fig. 2D), in agreement with the role of the flagellum in governing trypanosome morphogenesis [17].

The flagellum can be shorter because it is made too short, hence reflecting a defect in construction as predicted by the grow-and-lock model, but it could also be the case because it shortens after construction. To discriminate between these two possibilities, trypanosomes at a late stage of the cell cycle were investigated. These cells can easily be recognised because they possess two nuclei [24]. In control non-induced cells, the length of the new flagellum was ~15 µm whereas that of the old flagellum was ~20 µm (Fig. 3A, grey symbols on Fig. 3B) as expected because construction is not completed before cell division [24, 35]. This was confirmed by scanning electron microscopy of dividing cells: when the cleavage furrow was visible, the length of the new flagellum was shorter than that of the old one (Fig. 3C). In induced *KIN2A2B*^{RNAi} cells, the average length of the new flagellum was around 7 µm, for all induction times examined and that difference was statistically significant (Fig. 3A, black symbols on Fig. 3B). Analysis by scanning electron microscopy revealed that the new flagellum is much shorter and that the daughter cell is smaller (Fig. 3D) compared to the non-induced cells (Fig. 3C). This implies that the new flagellum is made too short when the cell is about to divide and supports the first postulate of the "grow and lock model": reducing the growth rate impacts on the length of the flagellum.

Presence of soluble tubulin does not support the limited cytoplasmic pool model

The shorter flagellum length could also be explained if the amount of soluble tubulin was more limited, for example because of the shorter cell size. In this were true, regulation of flagellum length could be explained by the model of the limiting pool of cytoplasmic components [36]. To challenge this model, the amount of soluble tubulin was determined using cell fractionation in detergent to separate a cytoskeletal and a soluble fraction [37]. Analysis non-induced *KIN2A2B*^{RNAi} cells demonstrated the existence of a low-abundance pool of soluble tubulin (Fig. S4) in agreement with previous studies [38]. A similar (possibly even more abundant) pool of soluble tubulin was found in *KIN2A2B*^{RNAi} cells after RNAi knockdown (Fig. S4). We conclude that the amount of soluble tubulin is not the limiting factor that would cause flagella to be shorter in *KIN2A2B*^{RNAi} cells after RNAi knockdown.

Evidence for flagellum locking after cell division is not compatible with the balance-point model

The grow-and-lock model implies that the mature flagellum is locked in a stable state that prevents further elongation or shortening. Although this is supported by the maintenance of flagellum length in the absence of IFT [19], the presence of a shorter mature flagellum of *KIN2A2B*^{RNAi} cells offers the possibility to bring more direct evidence. *KIN2A2B*^{RNAi} cells were grown in RNAi conditions for 6 days, resulting in the presence of short flagella as observed above. Tetracycline was washed out, leading to expression of fresh KIN2A and KIN2B and restoring IFT (Fig. 4A). The return of IFT trafficking in old and new flagella was monitored in live cells by the presence of a fusion protein between mNeonGreen [39] and IFT81 expressed from the endogenous *IFT81* locus [40]. After 16 hours without tetracycline, the frequency of IFT is increased by ~2-fold in both the new and the mature

flagellum (Table 2). This was confirmed by immunofluorescence staining with an anti-IFT172 antibody that revealed close to normal signal in both flagella (Fig. 4B). This shows that new IFT proteins have access to the mature flagellum in addition to the new one.

The length of each flagellum was measured using the Mab25 axonemal staining in induced and "de-induced" conditions. In induced conditions, the average length of the old flagellum was 14.2 ± 4.1 µm (black squares, Fig. 4C) whereas that of the new one was 8.25 ± 3.1 µm (black circles, Fig. 4C), as previously observed (Fig. 3B). Strikingly, the length of the old flagellum remained unchanged at 13.9 ± 4.08 µm (grey squares, Fig. 4C). This demonstrates that a 2-fold increase in IFT cannot rescue flagellum length after maturation. We interpret this result as evidence that the mature flagellum is locked. This also proves that the balance point model between assembly and disassembly does not apply to this type of flagellum since this model would predict an elongation of the flagellum upon increase of the IFT frequency [9].

The *T. brucei* flagellum is attached to the cell body via a sophisticated cytoskeletal network [41] and this could provide an original way to control flagellum length. This hypothesis is somehow contradicted by the fact that mutants with defects in the adhesion machinery assemble detached flagella of apparently normal length [42-46]. However, these flagella are completely detached from the cell body with the exception of the anchoring via the flagellar pocket and might be regulated differently compared to $KIN2A2B^{RNAi}$ cells where the short flagella are properly attached to the cell body. The "de-induction" experiment provides a way to challenge this model directly because at the time of tetracycline wash out, cells exhibit a short cell body. If this is a limiting factor, it should prevent further elongation of the new flagellum since it is formed on a short cell body. Measurements of the length of the new flagellum in de-induced cells contradicted this model. Indeed, the length of the new flagellum was 11.7 ± 3.9 µm instead of 8.25 ± 3.1 µm (Fig. 4C, grey circles). Examining the

ratio between the length of the new and the old flagellum revealed further interesting observations (Fig. 4D, grey circles). In close to one third of de-induced cells (16/55), the new flagellum was longer than the mature one; something that was never observed in induced *KIN2A2B*^{RNAi} cells (Fig. 4D, black circles) or in control cells [26]. Several of these cells grew flagella that extended well beyond the cell body (Fig. S5). We conclude that flagellum length is not controlled by the size of the cell body.

The locking event is initiated prior cell division

Having brought further evidence for flagellum locking, we next investigated the second postulate of the grow-and-lock model. It says that a timely controlled event should lead to a modification that locks the flagellum and prevents further elongation or shortening. Since flagellum assembly is intimately linked with the progression through the cell cycle in trypanosomes as in other protists [24, 47, 48], we propose that the locking event is controlled by a cell cycle-dependent mechanism rather than at the flagellum level. When a procyclic trypanosome divides, the new flagellum has reached ~80% of the length of the old flagellum meaning that elongation continues up to 20 µm in the daughter cell inheriting that flagellum. Post-division elongation has been experimentally proven but not quantified so far [49] and the events leading to its arrest are unknown. Arrest of flagellum growth could happen instantly or could be triggered by a specific signal that would be effective after a lag phase. In the first hypothesis (sharp arrest), flagellum elongation would be blocked when the flagellum becomes mature at some point after cell division. In the second hypothesis (delayed arrest), the signal leading to flagellum locking could happen prior or after cell division.

Whilst measuring the length of the new flagellum in *KIN2A2B*^{RNAi} cells (7 µm, see above), we noticed that the old flagellum of the same cells was almost twice longer (12 µm, black symbols, Fig. 3B), but albeit shorter than normal (20 µm). This could be explained by

the first hypothesis if the flagellum keeps its slow growth rate after cell division until the locking event occurs. But it could also be explained with the second model if the locking signal is triggered before division and blocks flagellum elongation later on. Therefore, this result does not discriminate between the two hypotheses.

To tease apart the mechanism responsible for the locking of the flagellum, cell division was inhibited. If the locking event takes place after division, it should be possible to restore normal flagellum length since flagellum growth should continue unabated. If it were initiated before cell division, only limited growth would be possible after activation of the signal. *KIN2A2B*^{RNAi} cells were grown in the presence of 10 mM teniposide, a drug that interferes with mitochondrial DNA segregation but neither with basal body duplication nor with flagellum elongation [50]. This resulted in the expected arrest of cell division that is clearly visible on the growth curve (Fig. S6). *KIN2A2B*^{RNAi} cells induced for 5 days were incubated in the presence of 10 mM teniposide. After incubation, cells were fixed and processed for IFA with the axonemal marker Mab25 whilst DNA was stained with DAPI. In controls without teniposide, the mitochondrial DNA segregated normally and cells progressed to the typical pattern with 2 kinetoplasts and 2 nuclei preceding cell division (Fig. 5A, top panels). By contrast, kinetoplasts failed to fully segregate in the presence of teniposide (Fig. 5A, bottom panels, white arrow), inhibiting cell division. In the absence of teniposide, the ratio between the length of the new and the old flagellum in induced *KIN2A2B*^{RNAi} cells was about 60% (Fig. 5B, light grey), in agreement with previous measurements (Fig. 3B). Remarkably, after 16 hours of incubation with teniposide, the ratio was close to 100%, meaning that the length of the new flagellum had reached the length of the old flagellum at ~12 µm but had failed to reach the normal 20 µm (Fig. 5B, dark grey, left bars). However, this short length could be due to slow elongation and not to a locking event. *KIN2A2B*^{RNAi} cells were therefore incubated for 24 hours in the presence of teniposide. These extra 8 hours

in teniposide did not result in an increase of new flagellum length that remained stuck at 12 µm (Fig. 5A, bottom panels & Fig. 5B, dark grey, right bars). We conclude that the signal for the locking event is triggered prior cell division and impacts elongation definitely.

One could consider that *KIN2A2B*^{RNAi} cells behave differently than wild-type cells for whatever reasons (shorter flagellum length, shorter cell size, reduced motility) and this might not reflect the normal situation. Therefore, we analysed the impact of an inhibition of cell division in wild-type cells. If the model is true, blocking cell division should result in an increase of the new flagellum from 80% (length of the new flagellum in wild-type cells) to 100% of the length of the old flagellum. In the absence of teniposide, the ratio between new and old flagella in cells about to divide was close to 80% as expected [26, 35](Fig. S7A, top panels and S7B, light grey bars). After incubation with teniposide, the length of the new flagellum reached that of the old flagellum but did not elongate further (Fig. S7A, bottom panels and S7B, dark grey bars). We conclude that when cytokinesis is blocked upon inhibition of mitochondrial DNA segregation, the signal that locks flagellum length is still present. This shows that this signal is triggered prior to cell division.

A molecular marker to monitor flagellum maturation

The last element of the grow-and-lock model implies that a modification of the flagellum takes place preventing further elongation. The data above indicate this must be progressive since it is initiated prior cell division and leads to an elongation arrest only after division. We therefore searched for candidate molecules that accumulate towards the late phase of flagellum elongation and could serve as markers for flagellum maturation. The FLAM8 protein appeared as an attractive candidate. It is a large protein (3,075 amino acids) of unknown function that was discovered in a proteomic study of purified trypanosome flagella [35]. FLAM8 is abundant at the distal tip of mature flagella and detected in very low

concentrations at the first stages of flagellum construction. However, its amount increases during elongation to reach 40% of that of the old flagellum just prior cell division [35]. It means that a significant increase must happen after cell division, which is compatible with the findings above.

If FLAM8 is indeed a marker of flagellum maturation, it should accumulate in the new flagellum of teniposide-treated cells. Therefore, cell division was inhibited using teniposide in induced *KIN2A2B*^{RNAi} cells exactly as above. Cells were fixed and stained by IFA with an anti-FLAM8 antibody, the Mab25 antibody as an axonemal marker, and DAPI to label DNA. When induced *KIN2A2B*^{RNAi} cells were not treated with teniposide, FLAM8 was abundant at the tip of the old flagellum, but was present in very low amounts or below detection level in the new flagellum (Fig. 6A, top panels). By contrast, in cells treated with teniposide for 24 hours, the new flagellum had elongated further as described above and the FLAM8 signal at its tip was much brighter and looked similar to that at the tip of the mature flagellum (Fig 6A, bottom panels). A circular region of interest was defined around the tip of the new and the old flagella and the total amount of fluorescence was quantified. In untreated induced *KIN2A2B*^{RNAi} cells at an advanced step of their cell cycle, the ratio of FLAM8 signal intensities between the new and the old flagellum was close to 60% (Fig. 6B, light grey). However, for induced cells treated with teniposide (where the new flagellum reached the length of the old flagellum), the FLAM8 ratio increased to 100% (Fig. 6B, dark grey). This difference was statistically significant.

We conclude that maturation of the new flagellum is initiated towards the end of the cell cycle and has an impact in the daughter cell after division. When cytokinesis is inhibited, maturation is triggered but because flagellum elongation is slower in induced *KIN2A2B*^{RNAi} cells due to the reduced IFT trafficking, the locking event took place too early, therefore preventing the new flagellum to reach the normal length of 20 µm. We conclude that these

results support the last point of the grow-and-lock model that implied that the mature flagellum should be different from the elongating flagellum.

DISCUSSION

In the grow-and-lock model proposed here, the flagellum shows a linear growth rate until a signal triggers a modification that blocks further elongation or shortening (Fig. 7A). The flagellum is now ready for its final function and its length is not modified anymore. In such a model, a cell can produce a shorter flagellum either by a slower growth rate (Fig. 7A, magenta curve) or by an earlier initiation of the locking event (Fig. 7B, magenta). Conversely, a longer flagellum can be constructed using a faster growth rate (Fig. 7A, green curve) or by delaying the timing of maturation (Fig. 7B, green). One could also consider that both parameters can be shifted together to achieve a different length. In this manuscript, we have exploited the *KIN2A2B*^{RNAi} cells that assemble shorter flagella to provide experimental evidence for the grow-and-lock model. First, we have shown that the mature flagellum is indeed locked since it does not elongate despite an increase of 2-fold in IFT trafficking in the de-induction experiment. This result adds up to the fact that the mature flagellum does not shorten in the absence of IFT [19]. We also reveal that FLAM8 can be considered as a molecular marker of mature flagella present at the distal end of the axoneme and whose high concentration reflects the state of maturation independent of the length of the flagellum. Second, we have shown that the signal for the locking event takes place prior cell division. Indeed, blocking mitochondrial DNA segregation with teniposide and hence cell division allows the flagellum of *KIN2A2B*^{RNAi} cells to elongate for a few microns but is followed by maturation and acquisition of a strong FLAM8 signal. Rising the incubation time in teniposide from 16 to 24 hours did not result in further increase in flagellum length, showing that it is definitely locked. Finally, a reduction of IFT frequency leads to a slower growth rate and results in the formation of a shorter flagellum, as predicted by the model (Fig. 7).

Importantly, the experiments reported here do not support other possible models for length control. First, the presence of a soluble pool of tubulin in control cells and in induced

KIN2A2B^{RNAi} cells that exhibit short flagella does not support the model based on control of flagellum length by a depletion of the pool of components [36]. Second, the fact that the short mature flagellum does not elongate despite a 2-fold augmentation of IFT trafficking in de-induced *KIN2A2B*^{RNAi} cells contradicts the balance point-model [9]. Third, the ability of *KIN2A2B*^{RNAi} cells to assemble fairly long new flagella that grow beyond the short cell body demonstrates that a control via the cytoskeletal attachment zone system [41] cannot explain the results either.

By contrast, the grow-and-lock model is so far the only one that is compatible with the experimental data. The principle is fairly simple since it relies on a linear growth rate and a locking event initiated prior cell division. There is no need to modulate the construction rate but this requires a sufficient supply of IFT proteins to ensure a regular increase of IFT trains in the flagellum and maintain a constant delivery rate of tubulin. This is in agreement with the fact that the amount of IFT proteins in the cell body largely exceeds that in the flagellum [18, 27, 51]. Moreover, the amount of *IFT* gene transcripts increases during flagellum assembly, followed closely by mRNA from genes coding for axonemal proteins [52, 53]. Examination of mouse photoreceptors during differentiation also indicates a significant amount of IFT proteins in the cell body in addition to the cilium [15, 54].

Here, we have shown that the event leading to the maturation of the flagellum is linked to the cell cycle timing and is triggered prior trypanosome division. This could also be the case of multiple protists where flagella are assembled during nuclear mitosis whilst maintaining flagella assembled in the previous generation(s) [24, 47, 48, 55]. The signal being activated before cell division, the cell commits to flagellum maturation even if it practically takes place only in the daughter cell. However, it is not directly controlled by cell division, since its inhibition by the teniposide treatment still allows maturation to occur, as well as elongation arrest.

This model has potential for cilia and flagella that do not disassemble their microtubules after assembly and maturation. Locking the length of the axoneme in a mature state could have significant advantages for cellular functions. Protein turnover costs energy and this would dispense the cell of a potentially costly maintenance process. A maybe more significant advantage may be found in the fact that cilia and flagella are central elements in the morphogenesis of the three cell types discussed here. In trypanosomes, the flagellum is attached along the length of the cell body from the onset of assembly. Some stages even use a flagella connector to position the new flagellum alongside the existing one [56]. The flagellum actually guides cell morphogenesis and defines the axis of cytokinesis [17, 44]. In spermatozoa, the axoneme of the flagellum is fully elongated before the cascade of morphogenetic events leading the emergence of the typical elongated shape of the cell body. These occur in a precise manner and are articulated around the flagellum [13, 57]. In photoreceptors, the large outer segment develops from the cilium [58] and is actually derived from the fusion of ectosomes that originated from it [59]. In all three situations, one could imagine the requirement of a stable axoneme both to ensure correct morphogenesis and to fulfil specific cell function after complete differentiation.

Locking the mature flagellum could help the cell to discriminate the new flagellum (that elongates) from the mature flagellum (that does not). Recent evidence indicates that the two flagella differ not only by their length but also by their content [35, 60]. This could be particularly helpful during differentiation steps where the new flagellum could perform a different function in the daughter cell [22, 23]. The situation is very different from the green algae *Chlamydomonas* that contains two flagella of normally equivalent length. When only one of them is severed, the remaining ones shortens while the severed one starts to grow again up to a point where both flagella grow at the same rate [61]. This implies an exchange of

information between the two flagella, something that was not observed in *T. brucei* where the two flagella function independently.

What could be the nature of the locking event that prevents further elongation of axoneme microtubules so stable? Several hypotheses can be put forward. First, the addition of a cap at the tip of microtubule doublets could be sufficient to prevent further assembly or disassembly. The identification of the distal tip FLAM8 protein as a marker of maturation goes along this line but it does not necessarily mean that this protein inhibits elongation. So far, a cap structure has not been detected on electron micrographs of *T. brucei* procyclic flagella [62] but the morphology of the axoneme tip looks very different between growing and mature flagella: whilst it looks disorganised in elongating flagella with some microtubule doublets very close to the central pair and others further away and in contact with the membrane, it is nicely and regularly structured in mature ones [63]. A cap at the tip could also protect against the action of the depolymerising kinesin 13 that has been connected to flagellum length control in the related protists *Leishmania major* [64] or *Giardia intestinalis* [65] but whose contribution appears minor in *T. brucei* [66]. A second possibility is the level of some post-translational modifications of tubulin that could alter the dynamics of microtubules. For example, the tip of the growing flagellum contains a large amount of tyrosinated tubulin that is not detected in the mature flagellum [67]. One could imagine that exhaustive detyrosination protects the axoneme from disassembly. By contrast, the totality of trypanosome tubulin being acetylated, a direct role of tubulin acetylation sounds unlikely [68]. Finally, the locking event could take place at the level of the base of the flagellum, for example by preventing access of fresh tubulin to the mature organelle. However, the de-induction experiment revealed that new IFT proteins were able to enter the mature flagellum, showing that access remained available, at least for this category of proteins. Yet, this was not accompanied by an increase in flagellum length. The membrane protein arginine kinase 3 also

has access to the mature flagellum since RNAi experiments showed it undergoes complete turnover in four hours [35]. Nevertheless, it remains to be seen if tubulin itself can access the old flagellum. Due to the failure of tagged tubulin to incorporate trypanosome microtubules [69, 70], it is not technically feasible to address this question.

The maturation/locking could be reversible in case the organelle needs to be modified, for example during a differentiation process [71], as recently demonstrated in the related parasite *Trypanosoma congolense* where shortening of the flagellum takes place during the transition between a free-swimming stage to an attached stage in culture conditions [72]. One could imagine that a structural cap is removed or that some post-translational modifications of tubulin are reverted, for example via the action of specific enzymes [73]. In mammalian cells, cilia are usually assembled after mitosis (or meiosis) in the so-called G0 phase of the cell cycle. If post-translational modifications are involved, the enzyme in charge could be expressed from this time point to progressively act on microtubules and finally inhibit assembly. Intriguingly, a "decapitation" process removes the distal end of the primary cilium in mouse embryonic fibroblasts as well as a large amount of IFT-B proteins before the organelle is resorbed [74].

Timing information for the locking event could come from the process of cell differentiation. We note that in both spermatozoa and photoreceptors, assembly of the cilium is one of the first steps in morphological differentiation [13, 59]. Alternatively, the timing of maturation could be controlled at the level of the flagellum once it reaches a certain length, via a length sensor. This possibility remains open via the time-of-flight model whereby a sensing molecule traffics in association with IFT proteins and undergoes some modification in the flagellum. As the flagellum elongates the time spent for a trip increases and the proportion of modified sensor could become high enough to trigger the locking event. This model had

been tested in *Chlamydomonas* but was not supported by experimental evidence in this organism [75]. In induced *KIN2A2B*^{RNAi} cells, the speed of IFT is reduced by ~30%, meaning that the time spent in the flagellum increases, what could trigger a premature locking event when the flagellum reaches 70% of the theoretical length. The length of the mature flagellum in induced *KIN2A2B*^{RNAi} cells is compatible with this result. The grow-and-lock model could therefore function with a length sensor system, as proposed in other organisms with more dynamic flagella [3, 76]. This simple model could therefore be suitable for different types of cilia and flagella with different options for the control of the growth rate and for both the mode and the timing of maturation of the organelle.

ACKNOWLEDGEMENTS

We acknowledge Derrick Robinson (Bordeaux, France), Paul McKean (Lancaster, UK) and Robert Lee Douglas (Berkeley, USA) for generous gifts of antibodies and Linda Kohl (Paris, France) for critical reading of the manuscript. We thank Adeline Mallet for the mNG::IFT81 cell line. We are thankful to the Ultrastructural BioImaging Plateforme for providing access to their equipment. E.B. is supported by fellowships from French National Ministry for Research and Technology (doctoral school CDV515) and from La Fondation pour la Recherche Médicale (FRM) (FDT20170436836). B.M. was supported by a Roux post-doctoral fellowship from the Institut Pasteur. This work is funded by ANR grants (11-BSV8-016 and 14-CE35-0009-01), by a French Government Investissement d'Avenir programme, Laboratoire d'Excellence "Integrative Biology of Emerging Infectious Diseases" (ANR-10-LABX-62-IBEID) and by La Fondation pour la Recherche Médicale (Equipe FRM DEQ20150734356). The funders had no role in the study design, data collection and analysis, decision to publish or preparation of the manuscript.

AUTHOR CONTRIBUTIONS

E.B., B.M., B.R. & P.B. conceived and designed the experiments; E.B., B.M. and T.B. performed the experiments; T.B. prepared the figures, E.B. and P.B. wrote the manuscript. All authors commented on the manuscript.

DECLARATION OF INTEREST

The authors declare no competing financial interests.

REFERENCES

1. Broekhuis, J.R., Leong, W.Y., and Jansen, G. (2013). Regulation of cilium length and intraflagellar transport. International review of cell and molecular biology *303*, 101-138.
2. Kozminski, K.G., Johnson, K.A., Forscher, P., and Rosenbaum, J.L. (1993). A motility in the eukaryotic flagellum unrelated to flagellar beating. Proc Natl Acad Sci U S A *90*, 5519-5523.
3. Wren, K.N., Craft, J.M., Tritschler, D., Schauer, A., Patel, D.K., Smith, E.F., Porter, M.E., Kner, P., and Lechtreck, K.F. (2013). A differential cargo-loading model of ciliary length regulation by IFT. Current biology : CB *23*, 2463-2471.
4. Craft, J.M., Harris, J.A., Hyman, S., Kner, P., and Lechtreck, K.F. (2015). Tubulin transport by IFT is upregulated during ciliary growth by a cilium-autonomous mechanism. J Cell Biol *208*, 223-237.
5. Prevo, B., Scholey, J.M., and Peterman, E.J.G. (2017). Intraflagellar transport: mechanisms of motor action, cooperation, and cargo delivery. FEBS J *284*, 2905-2931.
6. Ludington, W.B., Ishikawa, H., Serebrenik, Y.V., Ritter, A., Hernandez-Lopez, R.A., Gunzenhauser, J., Kannegaard, E., and Marshall, W.F. (2015). A systematic comparison of mathematical models for inherent measurement of ciliary length: how a cell can measure length and volume. Biophys J *108*, 1361-1379.
7. Adl, S.M., Simpson, A.G., Lane, C.E., Lukes, J., Bass, D., Bowser, S.S., Brown, M.W., Burki, F., Dunthorn, M., Hampl, V., et al. (2012). The revised classification of eukaryotes. J Eukaryot Microbiol *59*, 429-493.
8. Marshall, W.F., and Rosenbaum, J.L. (2001). Intraflagellar transport balances continuous turnover of outer doublet microtubules: implications for flagellar length control. J Cell Biol *155*, 405-414.
9. Engel, B.D., Ludington, W.B., and Marshall, W.F. (2009). Intraflagellar transport particle size scales inversely with flagellar length: revisiting the balance-point length control model. J Cell Biol *187*, 81-89.
10. Liang, Y., Pang, Y., Wu, Q., Hu, Z., Han, X., Xu, Y., Deng, H., and Pan, J. (2014). FLA8/KIF3B phosphorylation regulates kinesin-II interaction with IFT-B to control IFT entry and turnaround. Developmental cell *30*, 585-597.
11. Chien, A., Shih, S.M., Bower, R., Tritschler, D., Porter, M.E., and Yildiz, A. (2017). Dynamics of the IFT machinery at the ciliary tip. eLife *6*.
12. Hao, L., Thein, M., Brust-Mascher, I., Civelekoglu-Scholey, G., Lu, Y., Acar, S., Prevo, B., Shaham, S., and Scholey, J.M. (2011). Intraflagellar transport delivers tubulin isotypes to sensory cilium middle and distal segments. Nature cell biology *13*, 790-798.
13. San Agustin, J.T., Pazour, G.J., and Witman, G.B. (2015). Intraflagellar transport is essential for mammalian spermiogenesis but is absent in mature sperm. Molecular biology of the cell *26*, 4358-4372.
14. Besharse, J.C., and Hollyfield, J.G. (1979). Turnover of mouse photoreceptor outer segments in constant light and darkness. Invest Ophthalmol Vis Sci *18*, 1019-1024.
15. Jiang, L., Wei, Y., Ronquillo, C.C., Marc, R.E., Yoder, B.K., Frederick, J.M., and Baehr, W. (2015). Heterotrimeric kinesin-2 (KIF3) mediates transition zone and axoneme formation of mouse photoreceptors. J Biol Chem *290*, 12765-12778.

16. Vincensini, L., Blisnick, T., Bertiaux, E., Hutchinson, S., Georgikou, C., Ooi, C.P., and Bastin, P. (2017). Flagellar incorporation of proteins follows at least two different routes in trypanosomes. Biol Cell.
17. Kohl, L., Robinson, D., and Bastin, P. (2003). Novel roles for the flagellum in cell morphogenesis and cytokinesis of trypanosomes. Embo J *22*, 5336-5346.
18. Absalon, S., Blisnick, T., Kohl, L., Toutirais, G., Dore, G., Julkowska, D., Tavenet, A., and Bastin, P. (2008). Intraflagellar transport and functional analysis of genes required for flagellum formation in trypanosomes. Molecular biology of the cell *19*, 929-944.
19. Fort, C., Bonnefoy, S., Kohl, L., and Bastin, P. (2016). Intraflagellar transport is required for the maintenance of the trypanosome flagellum composition but not its length. Journal of cell science *129*, 3026-3041.
20. Rotureau, B., Subota, I., and Bastin, P. (2011). Molecular bases of cytoskeleton plasticity during the Trypanosoma brucei parasite cycle. Cell Microbiol *13*, 705-716.
21. Van Den Abbeele, J., Claes, Y., van Bockstaele, D., Le Ray, D., and Coosemans, M. (1999). Trypanosoma brucei spp. development in the tsetse fly: characterization of the post-mesocyclic stages in the foregut and proboscis. Parasitology *118*, 469-478.
22. Sharma, R., Peacock, L., Gluenz, E., Gull, K., Gibson, W., and Carrington, M. (2008). Asymmetric cell division as a route to reduction in cell length and change in cell morphology in trypanosomes. Protist *159*, 137-151.
23. Rotureau, B., Subota, I., Buisson, J., and Bastin, P. (2012). A new asymmetric division contributes to the continuous production of infective trypanosomes in the tsetse fly. Development *139*, 1842-1850.
24. Sherwin, T., and Gull, K. (1989). The cell division cycle of Trypanosoma brucei brucei: timing of event markers and cytoskeletal modulations. Philos Trans R Soc Lond B Biol Sci *323*, 573-588.
25. Bastin, P., MacRae, T.H., Francis, S.B., Matthews, K.R., and Gull, K. (1999). Flagellar morphogenesis: protein targeting and assembly in the paraflagellar rod of trypanosomes. Mol Cell Biol *19*, 8191-8200.
26. Robinson, D.R., Sherwin, T., Ploubidou, A., Byard, E.H., and Gull, K. (1995). Microtubule polarity and dynamics in the control of organelle positioning, segregation, and cytokinesis in the trypanosome cell cycle. J Cell Biol *128*, 1163-1172.
27. Buisson, J., Chenouard, N., Lagache, T., Blisnick, T., Olivo-Marin, J.C., and Bastin, P. (2013). Intraflagellar transport proteins cycle between the flagellum and its base. Journal of cell science *126*, 327-338.
28. Tyler, K.M., Matthews, K.R., and Gull, K. (2001). Anisomorphic cell division by African trypanosomes. Protist *152*, 367-378.
29. Huet, D., Blisnick, T., Perrot, S., and Bastin, P. (2014). The GTPase IFT27 is involved in both anterograde and retrograde intraflagellar transport. eLife *3*, e02419.
30. Shaner, N.C., Campbell, R.E., Steinbach, P.A., Giepmans, B.N., Palmer, A.E., and Tsien, R.Y. (2004). Improved monomeric red, orange and yellow fluorescent proteins derived from Discosoma sp. red fluorescent protein. Nature biotechnology *22*, 1567-1572.
31. Bhogaraju, S., Cajanek, L., Fort, C., Blisnick, T., Weber, K., Taschner, M., Mizuno, N., Lamla, S., Bastin, P., Nigg, E.A., et al. (2013). Molecular basis of tubulin transport within the cilium by IFT74 and IFT81. Science *341*, 1009-1012.
32. Julkowska, D., and Bastin, P. (2009). Tools for analyzing intraflagellar transport in trypanosomes. Methods Cell Biol *93*, 59-80.

33. Douglas, R., Haltiwanger, B., Wu, H., Jeng, R., Mancuso, J., Cande, Z., and Welch, M. (2018). Trypanosomes have divergent kinesin-2 proteins that function differentially in IFT, cell division, and motility. BioRxiv.
34. Wang, Z., Morris, J.C., Drew, M.E., and Englund, P.T. (2000). Inhibition of trypanosoma brucei gene expression by RNA interference using an integratable vector with opposing T7 promoters. J Biol Chem *275*, 40174-40179.
35. Subota, I., Julkowska, D., Vincensini, L., Reeg, N., Buisson, J., Blisnick, T., Huet, D., Perrot, S., Santi-Rocca, J., Duchateau, M., et al. (2014). Proteomic analysis of intact flagella of procyclic Trypanosoma brucei cells identifies novel flagellar proteins with unique sub-localization and dynamics. Molecular & cellular proteomics : MCP *13*, 1769-1786.
36. Goehring, N.W., and Hyman, A.A. (2012). Organelle growth control through limiting pools of cytoplasmic components. Current biology : CB *22*, R330-339.
37. Robinson, D., Beattie, P., Sherwin, T., and Gull, K. (1991). Microtubules, tubulin, and microtubule-associated proteins of trypanosomes. Methods in enzymology *196*, 285-299.
38. Schneider, A., Sherwin, T., Sasse, R., Russell, D.G., Gull, K., and Seebeck, T. (1987). Subpellicular and flagellar microtubules of Trypanosoma brucei brucei contain the same alpha-tubulin isoforms. J Cell Biol *104*, 431-438.
39. Shaner, N.C., Lambert, G.G., Chammas, A., Ni, Y., Cranfill, P.J., Baird, M.A., Sell, B.R., Allen, J.R., Day, R.N., Israelsson, M., et al. (2013). A bright monomeric green fluorescent protein derived from Branchiostoma lanceolatum. Nat Methods *10*, 407-409.
40. Bertiaux, E., Mallet, A., Fort, C., Blisnick, T., Bonnefoy, S., Jung, J., Lemos, M., Vaughan, S., Marco, S., Trépout, S., et al. (2018). Bidirectional intraflagellar transport is restricted to only two microtubule doublets in the trypanosome flagellum. BioRxiv.
41. Sunter, J.D., and Gull, K. (2016). The Flagellum Attachment Zone: 'The Cellular Ruler' of Trypanosome Morphology. Trends in parasitology.
42. LaCount, D.J., Barrett, B., and Donelson, J.E. (2002). Trypanosoma brucei FLA1 is required for flagellum attachment and cytokinesis. J Biol Chem *277*, 17580-17588.
43. Rotureau, B., Blisnick, T., Subota, I., Julkowska, D., Cayet, N., Perrot, S., and Bastin, P. (2014). Flagellar adhesion in Trypanosoma brucei relies on interactions between different skeletal structures in the flagellum and cell body. Journal of cell science *127*, 204-215.
44. Zhou, Q., Liu, B., Sun, Y., and He, C.Y. (2011). A coiled-coil- and C2-domain-containing protein is required for FAZ assembly and cell morphology in Trypanosoma brucei. Journal of cell science *124*, 3848-3858.
45. Sun, S.Y., Wang, C., Yuan, Y.A., and He, C.Y. (2013). An intracellular membrane junction consisting of flagellum adhesion glycoproteins links flagellum biogenesis to cell morphogenesis in Trypanosoma brucei. Journal of cell science *126*, 520-531.
46. Sunter, J.D., Benz, C., Andre, J., Whipple, S., McKean, P.G., Gull, K., Ginger, M.L., and Lukes, J. (2015). Modulation of flagellum attachment zone protein FLAM3 and regulation of the cell shape in Trypanosoma brucei life cycle transitions. Journal of cell science *128*, 3117-3130.
47. Dawson, S.C., and House, S.A. (2010). Life with eight flagella: flagellar assembly and division in Giardia. Curr Opin Microbiol *13*, 480-490.
48. Noel, C., Gerbod, D., Delgado-Viscogliosi, P., Fast, N.M., Younes, A.B., Chose, O., Roseto, A., Capron, M., and Viscogliosi, E. (2003). Morphogenesis during division and griseofulvin-induced changes of the microtubular cytoskeleton in the parasitic protist, Trichomonas vaginalis. Parasitol Res *89*, 487-494.

49. Farr, H., and Gull, K. (2009). Functional studies of an evolutionarily conserved, cytochrome b5 domain protein reveal a specific role in axonemal organisation and the general phenomenon of post-division axonemal growth in trypanosomes. Cell motility and the cytoskeleton *66*, 24-35.
50. Robinson, D.R., and Gull, K. (1991). Basal body movements as a mechanism for mitochondrial genome segregation in the trypanosome cell cycle. Nature *352*, 731-733.
51. Franklin, J.B., and Ullu, E. (2010). Biochemical analysis of PIFTC3, the Trypanosoma brucei orthologue of nematode DYF-13, reveals interactions with established and putative intraflagellar transport components. Mol Microbiol *78*, 173-186.
52. Morga, B., and Bastin, P. (2013). Getting to the heart of intraflagellar transport using Trypanosoma and Chlamydomonas models: the strength is in their differences. Cilia *2*, 16.
53. Archer, S.K., Inchaustegui, D., Queiroz, R., and Clayton, C. (2011). The cell cycle regulated transcriptome of Trypanosoma brucei. PloS one *6*, e18425.
54. Pazour, G.J., Baker, S.A., Deane, J.A., Cole, D.G., Dickert, B.L., Rosenbaum, J.L., Witman, G.B., and Besharse, J.C. (2002). The intraflagellar transport protein, IFT88, is essential for vertebrate photoreceptor assembly and maintenance. J Cell Biol *157*, 103-113.
55. Wheeler, R.J., Gluenz, E., and Gull, K. (2011). The cell cycle of Leishmania: morphogenetic events and their implications for parasite biology. Mol Microbiol *79*, 647-662.
56. Moreira-Leite, F.F., Sherwin, T., Kohl, L., and Gull, K. (2001). A trypanosome structure involved in transmitting cytoplasmic information during cell division. Science *294*, 610-612.
57. Leblond, C.P., and Clermont, Y. (1952). Definition of the stages of the cycle of the seminiferous epithelium in the rat. Ann N Y Acad Sci *55*, 548-573.
58. Molday, R.S., and Moritz, O.L. (2015). Photoreceptors at a glance. Journal of cell science *128*, 4039-4045.
59. Salinas, R.Y., Pearring, J.N., Ding, J.D., Spencer, W.J., Hao, Y., and Arshavsky, V.Y. (2017). Photoreceptor discs form through peripherin-dependent suppression of ciliary ectosome release. J Cell Biol *216*, 1489-1499.
60. Bonnefoy, S., Watson, C.M., Kernohan, K.D., Lemos, M., Hutchinson, S., Poulter, J.A., Crinnion, L.A., O'Callaghan, C., Hirst, R.A., Rutman, A., et al. (2018). Biallelic Mutations in LRRC56 encoding a protein associated with intraflagellar transport, cause mucociliary clearance and laterality defects. BioRxiv.
61. Rosenbaum, J.L., Moulder, J.E., and Ringo, D.L. (1969). Flagellar elongation and shortening in Chlamydomonas. The use of cycloheximide and colchicine to study the synthesis and assembly of flagellar proteins. J Cell Biol *41*, 600-619.
62. Woolley, D., Gadelha, C., and Gull, K. (2006). Evidence for a sliding-resistance at the tip of the trypanosome flagellum. Cell motility and the cytoskeleton *63*, 741-746.
63. Höög, J.L., Lacomble, S., O'Toole, E.T., Hoenger, A., McIntosh, J.R., and Gull, K. (2014). Modes of flagellar assembly in Chlamydomonas reinhardtii and Trypanosoma brucei. eLife *3*, e01479.
64. Blaineau, C., Tessier, M., Dubessay, P., Tasse, L., Crobu, L., Pages, M., and Bastien, P. (2007). A novel microtubule-depolymerizing kinesin involved in length control of a eukaryotic flagellum. Current biology : CB *17*, 778-782.
65. Dawson, S.C., Sagolla, M.S., Mancuso, J.J., Woessner, D.J., House, S.A., Fritz-Laylin, L., and Cande, W.Z. (2007). Kinesin-13 regulates flagellar, interphase, and mitotic microtubule dynamics in Giardia intestinalis. Eukaryotic cell *6*, 2354-2364.

66. Chan, K.Y., and Ersfeld, K. (2010). The role of the Kinesin-13 family protein TbKif13-2 in flagellar length control of Trypanosoma brucei. Mol Biochem Parasitol *174*, 137-140.
67. Sherwin, T., Schneider, A., Sasse, R., Seebeck, T., and Gull, K. (1987). Distinct localization and cell cycle dependence of COOH terminally tyrosinolated alpha-tubulin in the microtubules of Trypanosoma brucei brucei. J Cell Biol *104*, 439-446.
68. Schneider, A., Plessmann, U., and Weber, K. (1997). Subpellicular and flagellar microtubules of Trypanosoma brucei are extensively glutamylated. Journal of cell science *110 (Pt 4)*, 431-437.
69. Bastin, P., Bagherzadeh, Z., Matthews, K.R., and Gull, K. (1996). A novel epitope tag system to study protein targeting and organelle biogenesis in Trypanosoma brucei. Mol Biochem Parasitol *77*, 235-239.
70. Sheriff, O., Lim, L.F., and He, C.Y. (2014). Tracking the biogenesis and inheritance of subpellicular microtubule in Trypanosoma brucei with inducible YFP-alpha-tubulin. BioMed research international *2014*, 893272.
71. Ooi, C.P., and Bastin, P. (2013). More than meets the eye: understanding Trypanosoma brucei morphology in the tsetse. Frontiers in cellular and infection microbiology *3*, 1-12.
72. Peacock, L., Kay, C., Bailey, M., and Gibson, W. (2018). Shape-shifting trypanosomes: Flagellar shortening followed by asymmetric division in Trypanosoma congolense from the tsetse proventriculus. PLoS Pathog *14*, e1007043.
73. Gadadhar, S., Bodakuntla, S., Natarajan, K., and Janke, C. (2017). The tubulin code at a glance. Journal of cell science *130*, 1347-1353.
74. Phua, S.C., Chiba, S., Suzuki, M., Su, E., Roberson, E.C., Pusapati, G.V., Setou, M., Rohatgi, R., Reiter, J.F., Ikegami, K., et al. (2017). Dynamic Remodeling of Membrane Composition Drives Cell Cycle through Primary Cilia Excision. Cell *168*, 264-279 e215.
75. Ishikawa, H., and Marshall, W.F. (2017). Testing the time-of-flight model for flagellar length sensing. Molecular biology of the cell *28*, 3447-3456.
76. Cao, M., Meng, D., Wang, L., Bei, S., Snell, W.J., and Pan, J. (2013). Activation loop phosphorylation of a protein kinase is a molecular marker of organelle size that dynamically reports flagellar length. Proc Natl Acad Sci U S A *110*, 12337-12342.
77. Le Ray, D., Barry, J.D., Easton, C., and Vickerman, K. (1977). First tsetse fly transmission of the "AnTat" serodeme of Trypanosoma brucei. Ann Soc Belg Med Trop *57*, 369-381.
78. Brun, R., and Schonenberger (1979). Cultivation and in vitro cloning or procyclic culture forms of Trypanosoma brucei in a semi-defined medium. Short communication. Acta tropica *36*, 289-292.
79. Wirtz, E., Leal, S., Ochatt, C., and Cross, G.A. (1999). A tightly regulated inducible expression system for conditional gene knock-outs and dominant-negative genetics in Trypanosoma brucei. Mol Biochem Parasitol *99*, 89-101.
80. Redmond, S., Vadivelu, J., and Field, M.C. (2003). RNAit: an automated web-based tool for the selection of RNAi targets in Trypanosoma brucei. Mol Biochem Parasitol *128*, 115-118.
81. Kelly, S., Reed, J., Kramer, S., Ellis, L., Webb, H., Sunter, J., Salje, J., Marinsek, N., Gull, K., Wickstead, B., et al. (2007). Functional genomics in Trypanosoma brucei: a collection of vectors for the expression of tagged proteins from endogenous and ectopic gene loci. Mol Biochem Parasitol *154*, 103-109.

82. Burkard, G., Fragoso, C.M., and Roditi, I. (2007). Highly efficient stable transformation of bloodstream forms of Trypanosoma brucei. Mol Biochem Parasitol *153*, 220-223.
83. Absalon, S., Kohl, L., Branche, C., Blisnick, T., Toutirais, G., Rusconi, F., Cosson, J., Bonhivers, M., Robinson, D., and Bastin, P. (2007). Basal body positioning is controlled by flagellum formation in Trypanosoma brucei. PloS one *2*, e437.
84. Pradel, L.C., Bonhivers, M., Landrein, N., and Robinson, D.R. (2006). NIMA-related kinase TbNRKC is involved in basal body separation in Trypanosoma brucei. Journal of cell science *119*, 1852-1863.
85. Chenouard, N., Buisson, J., Bloch, I., Bastin, P., and Olivo-Marin, J.C. (2010). Curvelet analysis of kymograph for tracking bi-directional particles in flurescence microscopy images. International Conference on Image Processing, in press.
86. Subota, I., Rotureau, B., Blisnick, T., Ngwabyt, S., Durand-Dubief, M., Engstler, M., and Bastin, P. (2011). ALBA proteins are stage regulated during trypanosome development in the tsetse fly and participate in differentiation. Molecular biology of the cell *22*, 4205-4219.
87. Woods, A., Sherwin, T., Sasse, R., MacRae, T.H., Baines, A.J., and Gull, K. (1989). Definition of individual components within the cytoskeleton of Trypanosoma brucei by a library of monoclonal antibodies. Journal of cell science *93*, 491-500.
88. Adhiambo, C., Blisnick, T., Toutirais, G., Delannoy, E., and Bastin, P. (2009). A novel function for the atypical small G protein Rab-like 5 in the assembly of the trypanosome flagellum. Journal of cell science *122*, 834-841.

FIGURE LEGENDS

Figure 1. IFT trafficking during flagellum construction is compatible with a linear growth rate

(A) Still images of AnTat1.1E cells expressing a TdTomato::IFT81 from the endogenous locus. Subpanel 1 shows a cell with a single flagellum (Video S1) and subpanels 2-4 show cells at successive stages of flagellum construction (Videos S2-S4). Orange and white arrowheads indicate the new and the old flagellum, respectively. (B) Kymographs extracted from the corresponding videos where the X axis corresponds to flagellum length (horizontal scale bar, 2 μm) and the Y axis represents the elapsed time (vertical bar, 1s). (C) The ratio between the total TdT::IFT81 fluorescence intensity in the new and the old flagellum was calculated and plotted according to the length of the new flagellum. A linear correlation curve is indicated together with its R^2 coefficient. (D) The ratio between IFT rates (anterograde transport, magenta circles; retrograde transport, green circles) in the new flagellum and the old flagellum from the same cell was calculated and plotted according to the length of the new flagellum. Retrograde transport is more difficult to detect and data were only incorporated when the signal was sufficiently reliable. (E) Quantification of the ratio between the IFT frequency (anterograde transport, magenta circles; retrograde transport, green circles) in the new flagellum and the old flagellum in the same cell was calculated and plotted versus the length of the new flagellum. See Table 1 for total number of trains analysed.

Figure 2. Reduction of IFT train frequency impacts on flagellum length in *KIN2A2B^{RNAi}* cells.

(A) IFA of non-induced *KIN2A2B^{RNAi}* cells, or cells induced for 3 or 6 days as indicated, fixed in methanol, and stained with the Mab25 antibody to detect the axoneme (white). The top

panels show the phase-contrast image merged with DAPI (blue) and Mab25 signal (white). Scale bar: 10µm. The bottom panels show Mab25 staining (white) merged with DAPI (blue). (B) Dot plot showing flagellum length during the course of RNAi induction of *KIN2A2B*^{RNAi} cells including 100 uni-flagellated cells for each time point. The mean values are indicated with a bold segment. Statistically significant differences are indicated with two stars ($p<0.0001$). (C-D) Scanning electron microscopy analysis of a non-induced *KIN2A2B*^{RNAi} cell showing the typical trypanosome shape and length (C) and of two induced *KIN2A2B*^{RNAi} cells for 6 days with shorter flagella (D).

Figure 3. The new flagellum is built shorter upon reduction of IFT train frequency in *KIN2A2B*^{RNAi} cells.

(A) IFA images of non-induced and 6-day induced *KIN2A2B*^{RNAi} cells obtained after methanol fixation and staining with the Mab25 antibody labeling the axoneme (white). The top panels show the phase-contrast images merged with DAPI (cyan) and the Mab25 axonemal marker (red) and the bottom ones show the Mab25 signal (white) merged with DAPI (cyan). Scale bar: 10µm. (B) Dot plot showing the length of old and new flagella during the course of RNAi induction of *KIN2A2B*^{RNAi} measured in cells possessing 2 kinetoplasts and 2 nuclei (n= 50 for each time point). The mean values are indicated with a bold segment. Statistically significant differences are indicated with one ($p<0.001$) or two stars ($p<0.0001$). (C) Scanning electron microscopy pictures of non-induced (C) and induced *KIN2A2B*^{RNAi} cells after 6 days (D). The purple arrow indicates the cleavage furrow. Orange and white arrowheads show the new and the old flagellum, respectively.

Figure 4. De-induction of RNAi leads to an increase of IFT trafficking in *KIN2A2B*^{RNAi} cells but has no impact on the length of the mature flagellum.

(A) Schematic representation of the de-induction experiment. *KIN2A2B*^{RNAi} cells were grown in RNAi conditions for 6 days before extensive washings to remove tetracycline and returned to culture with (control) or without tetracycline (de-induced) for 16 hours. (B) IFA pictures of a de-induced *KIN2A2B*^{RNAi} cell undergoing cytokinesis, stained with the anti-IFT172 antibody and with the Mab25 antibody targeting the axoneme as indicated. The first image shows phase contrast and DAPI staining (cyan). The merged panel contains DAPI (cyan), Mab25 (white) and IFT172 (magenta) signals. Scale bar: 5µm. (C) Dot plot showing the length of old and new flagella in *KIN2A2B*^{RNAi} cells that were grown in RNAi conditions (left, black symbols) and in de-induced cells for 16 hours (grey symbols). This was measured in cells possessing 2 kinetoplasts and 2 nuclei (n=54 for induced cells and n=49 for de-induced cells). (D) Dot plot representing the ratio between the length of the new flagellum and that of the old flagellum. The mean values are indicated with a bold segment. Statistically significant differences are indicated with two stars ($p<0.0001$).

Figure 5. Inhibition of cell division impacts flagellar length.

(A) IFA pictures of 6-day induced *KIN2A2B*^{RNAi} cells that were left untreated (top panels) or treated for 24 hours with teniposide (bottom panels), stained with the Mab25 antibody targeting the axoneme (white) and DAPI labeling DNA (cyan). The left panels show the phase-contrast image merged with DAPI (cyan) and Mab25 signal (white). The right panels show the Mab25 signal (white) and DAPI (cyan). Orange and white arrowheads show the new and the old flagellum, respectively. The white arrow shows the bridge linking the kinetoplasts after treatment with teniposide. Scale bar: 5µm. (B) Ratio between the length of the new flagellum and the old flagellum for 6-day induced *KIN2A2B*^{RNAi} cells treated (dark bars) or not (white bars) with teniposide during 16 (left, one experiment) or 24 (right, three independent experiments with standard deviation) hours. For the 16 hour-experiment, n=40

for teniposide-treated cells and n=62 for the untreated control. For the 24 hour-experiment, n=112 for teniposide-treated cells and n=163 for the untreated control. Statistically significant differences are indicated with two stars ($p<0.0001$).

Figure 6. The event leading to flagellum maturation is triggered prior cell division.

(A) IFA pictures of 6 day-induced *KIN2A2B*^{RNAi} cells non-treated or treated for 24 hours with teniposide, fixed in methanol and stained using the Mab25 antibody to detect the axoneme (white), the anti-FLAM8 (magenta) and DAPI (cyan). The left panels show the phase-contrast image merged with DAPI (cyan), the anti-FLAM8 (magenta) and Mab25 antibody (white). The right panels show the anti-FLAM8 signal only (white). Orange and white arrowheads show the new and the old flagellum, respectively. The white circles are centered on the FLAM8 signal. Scale bar: 5µm. (B) Ratios between the FLAM8 fluorescent signal intensity in the new and the old flagellum in 6 day-induced *KIN2AB*^{RNAi} cells treated (n=109) or not (n=60) with teniposide during 24 hours. Two independent experiments are shown. Statistically significant differences are indicated with two stars ($p<0.0001$).

Figure 7. The grow-and-lock model to explain the control of flagellum length in *T. brucei*

(A) A slower (magenta) or faster (green) growth rate allows the production of shorter or longer flagella without having to change the timing of the locking event. (B) The flagellum elongates with a linear growth rate until a point where it is locked (arrow) and shows neither assembly nor disassembly. Keeping the same growth rate but triggering the locking event earlier (magenta) or later (green) will result in the formation of shorter or longer flagella.

STAR METHODS

Plasmids, cell lines, and culture conditions

The pleomorphic strain *T. brucei* AnTat1.1E [77] was used for transformation with p2675TdTIFT81. Cells were cultured in SDM79 medium [78] supplemented with hemin, 10% fetal bovine serum and 10mM glycerol. All the other procyclic *T. brucei* cell lines were derivatives of the strain 427 and grown in SDM79 medium with hemin and 10% fetal bovine serum. All the cells were cultivated at 27°C. The 29–13 cell line expressing the T7 RNA polymerase and the tetracycline-repressor has been described previously [79]. For generation of the *KIN2A2B*^{RNAi} cell line, a 489-nucleotide fragment of *KIN2A* (Tb927.11.13920) was amplified by PCR flanked by HindIII and XhoI sites and cloned in the compatible sites of the pZJM vector. The *KIN2B* (Tb 927.5.2090) fragment was generated by chemical synthesis by GeneCust Europe (Dudelange, Luxembourg). Genecust cloned these fragment into the pZJM vector [34], allowing tetracycline-inducible expression of dsRNA generating RNAi upon transfection in the 29-13 recipient cell line. The dsRNA is expressed from two tetracycline-inducible T7 promoters facing each other in the pZJM vector. Primers were selected using the RNAit algorithm to ensure that the fragment lacked significant identity to other genes to avoid cross-RNAi [80]. For generation of the *KIN2A2B*^{RNAi} expressing TdT::IFT81 cell line and AnTat1.1E expressing TdT::IFT81, the first 500 nucleotides of the *IFT81* gene (Gene DB number Tb927.10.2640) were chemically synthesised (GeneCust, Luxembourg) and cloned in frame with the TdTomato gene within the HindIII and ApaI sites of the p2675 vector [81]. The construct was linearised within the *IFT81* sequence with the enzyme XcmI and nucleofected [82] in the *KIN2A2B*^{RNAi} or the AnTat1.1E cell line, leading to integration by homologous recombination in the *IFT81* endogenous locus and to expression of the full-length coding sequence of IFT81 fused to TdTomato. To construct the

p2675mNeonGreenIFT81 plasmid, the *mNeonGreen* gene [39] was chemically synthesised (GeneCust, Luxembourg) with HindIII and ApaI site and cloned in the corresponding site of the p2675YFPIFT81 [31] to replace the *YFP* gene. The vector was linearised with XcmI and nucleofected in the *KIN2A2B*^{RNAi} cell line as described above. Transfectants were grown in media with the appropriate antibiotic concentration and clonal populations were obtained by limited dilution.

For de-induction experiments, *KIN2A2B*^{RNAi} cells were grown for 6 days in the presence of tetracycline and then washed in four times in SMD79 supplemented with serum and hemin before being returned to culture either in the presence of tetracycline (induced control) or in the absence of tetracycline (de-induced sample). For inhibition of cell division, teniposide (Sigma SML0609), a topoisomerase II inhibitor was dissolved in DMSO and added to trypanosome cultures at a final concentration of 200 µM [50] during 24 hours (*KIN2A2B*^{RNAi} strain) and 8 hours (wild-type strain). In the control flask, the same volume of DMSO was added (63 µL).

Scanning electron microscopy

For scanning electron microscopy, samples were fixed overnight at 4°C with 2.5% glutaraldehyde in 0.1 M cacodylate buffer (pH 7.2) and post-fixed in 2% OsO_4 in the same buffer. After serial dehydration, samples were dried at the critical point and coated with platinum according to standard procedures [83]. Observations were made in a JEOL 7600F microscope.

Immunofluorescence and live cell imaging

Cultured parasites were washed twice in SDM79 medium without serum or in Phosphate Buffer Saline (PBS), and spread directly onto poly-L-lysine coated slides. The slides were air-

dried for 10 min, fixed in methanol at −20°C for 30 s and rehydrated for 10 min in PBS. For immuno-detection, slides were incubated with primary antibodies diluted in PBS with 0.1% Bovine Serum Albumin (BSA) for 1 h at 37°C. Three washes of 10 min were performed and the secondary antibody diluted in PBS with 0.1% BSA was added to the slides. After an incubation of 45 min at 37°C, slides were washed three times in PBS for 10 min and DAPI (2 µg/µl) was added. Slides were mounted with coverslips using ProLong antifade reagent (Invitrogen). The antibodies used were the Mab25 monoclonal antibody recognising TbSAXO1, a protein found all along the trypanosome axoneme [84], an anti-IFT172 mouse monoclonal antibody diluted at 1/200 [18], an anti-FLAM8 rabbit polyclonal 1/500 (kind gift of Paul McKean, Lancaster University, UK). Subclass-specific secondary antibodies coupled to Alexa 488 and Cy3 (1/400; Jackson ImmunoResearch Laboratories, West Grove, PA) were used for double labelling. Sample observation was performed using a DMI4000 microscope equipped with a 100X NA 1.4 lens (Leica, Wetzlar, Germany) and images captured with an ORCA-03G Hamamatsu camera. Pictures were analyzed using ImageJ 1.47g13 software (National Institutes of Health, Bethesda, MD) and images were merged and superimposed using Adobe Photoshop CC. For fluorescence quantification, we have used the Raw Integrated Density values and removed the background at all these values. For live video microscopy, cells were covered with a coverslip and observed directly with the DMI4000 microscope at room temperature. Videos were acquired using an Evolve 512 EMCCD Camera (Photometrics, Tucson, AZ), driven by the Metavue acquisition software (Molecular Probes, Sunnyvale, CA). IFT trafficking was recorded at 100 (AnTat1.1E expressing TdT::IFT81) or 250 (*KIN2A2B*^{RNAi} expressing TdT::IFT81) milliseconds per frame during 30 seconds. Kymographs were extracted and analysed as described previously [27, 85]. For length measurements, the Mab25 staining of the axoneme was taken as reference using ImageJ. Statistical analyses were done with Kaleidagraph v4.5.2 using ANOVA test with

Turkey HSD (α=0.5). Graphs were drawn using Kaleidagraph v4.5.2. All errors correspond to the standard deviation of the population.

Western blot analysis

Cells were washed in PBS and boiled in Laemmli loading buffer before SDS-PAGE separation, loading 20 µg of total cell protein per lane. Proteins were transferred overnight at 25V at 4°C to polyvinylidene fluoride membranes (PVDF), then blocked with 5% skimmed milk in PBS-Tween 0.1% (PBST) and incubated with primary antibodies diluted in 1% milk and PBST. The anti-KIN2B (a kind gift of Robert L. Douglas, Berkeley)[33] serum was diluted 1/100. As loading controls, antibodies against ALBA proteins [86] diluted 1/500 were used. Three membrane washes were performed with PBST for 5 minutes. Species-specific secondary antibodies coupled to horseradish peroxidase (GE Healthcare) were diluted 1/20,000 in PBST containing 1% milk and incubated for 1 hour. Final detection was carried out using an enhanced chemoluminescence kit and a high performance chemoluminescence film according to manufacturer's instructions (Amersham, Piscataway, NJ).

For fractionation in detergent, cells were washed twice in PBS by 5 minutes at 500 *g* and the pellet was incubated for 2 minutes in Nonidet P-40 1% in PEM buffer in the presence of protease inhibitors (Sigma P8340). After centrifugation for 2 minutes at full speed, the supernatant (soluble fraction) was separated from the pellet (cytoskeletal fraction). Cells without treatment were used as control (total extract). Samples were loaded on gel and treated as above for transfer on membranes. Tubulin was detected with the TAT-1 monoclonal antibody [87] and IFT22 that was used here as a soluble marker was detected with a mouse anti-IFT22 antiserum [88].

SUPPLEMENTAL INFORMATION

Figure S1. Cartoons representing the trypanosome cell cycle in different conditions

(A) In wild-type conditions, a new flagellum elongates after duplication of the basal body. After mitosis, flagellum has grown to ~80% of its final length [24, 26]. One daughter cell inherits the old flagellum and the other one inherits the new flagellum after division. This one continues growing until it reaches the final length of 20 µm. (B) In *KIN2A2B*^{RNAi} cells, the new flagellum only reaches 7 µm at the time of cell division but elongates up to 12 µm until it matures in the next cell cycle. DNA is shown in dark blue whereas old and new flagella are shown in cyan and orange, respectively.

Figure S2. RNAi efficiently targets KIN2B at the protein level.

Total protein samples of non-induced and induced *KIN2A2B*^{RNAi} cells were prepared after the indicated number of days. Proteins were separated by SDS-PAGE, transferred to a PVDF membrane that was incubated with the anti-KIN2B (top picture) or the anti-ALBA that detects ALBA3 and ALBA4 as loading control (bottom picture).

Figure S3. The frequency of IFT trains is reduced in *KIN2A2B*^{RNAi} cells.

Live imaging of a non-induced (A) and a 6-day induced *KIN2A2B*^{RNAi} cell (B) expressing the TdT::IFT81 from its endogenous locus. Still images from Video S5 (A) and S6 (B) at the indicated time points showing the movement of IFT trains. White arrowheads indicate the successive position of anterograde IFT trains. Kymograph analyses from non-induced (C) and induced cells (D) show clear anterograde IFT traces that are highlighted in color. Note the

difference in frequency between non-induced and induced cells. Horizontal scale bar is 2µm and vertical scale bar is 2s.

Figure S4. A soluble pool of tubulin is available.

Samples from *KIN2A2B*^{RNAi} cells grown in non-induced or induced conditions for 8 days were run on gel, transferred to membranes and incubated with the indicated antibodies. Total protein samples, detergent-soluble and cytoskeletal fractions were analysed. Tubulin was detected with the TAT-1 monoclonal antibody whereas IFT22 (soluble marker) was detected with a mouse anti-IFT22 antiserum [88]. Tubulin is detected in the soluble pool in all conditions. Since the cytoskeletal pool is comparatively more abundant [38], a higher amount of protein was loaded to analyse the soluble pool alone (right panel). This confirmed the presence of a soluble pool of tubulin in both non-induced and induced conditions.

Figure S5. De-induction of RNAi in *KIN2A2B*^{RNAi} cells leads to the formation of longer new flagella that extend beyond the cell body.

IFA pictures of a de-induced *KIN2A2B*^{RNAi} cell undergoing cytokinesis, stained with the Mab25 antibody targeting the axoneme. The first image shows phase contrast and DAPI staining (cyan) and the second one shows the axoneme staining (white). White and orange arrowheads indicate the old and the new flagellum, respectively.

Figure S6. Teniposide blocks cell proliferation.

Growth curve of wild-type cells untreated (grey continuous line) or treated with teniposide for 24h (grey dotted line) and 6 day-induced *KIN2A2B*^{RNAi} cells untreated (cyan continuous line) or treated with teniposide (purple dotted line).

Figure S7. Inhibition of cell division and flagellum growth in wild-type cells

(A) IFA pictures of or wild-type cells that were left untreated (top panels) or treated for 24 hours with teniposide (bottom panels), stained with the Mab25 antibody targeting the axoneme (white) and DAPI labeling DNA (cyan). The left panels show the phase-contrast image merged with DAPI (cyan) and Mab25 signal (white). The right panels show the Mab25 signal (white) and DAPI (cyan). Orange and white arrowheads show the new and the old flagellum, respectively. The white arrows show the bridge linking the kinetoplasts after treatment with teniposide. Scale bar: 5µm. (B) Ratios between the length of the new flagellum and the old flagellum for wild-type cells treated (dark bars, n=150) or not (white bars, n=180) with teniposide during 8 hours. The results are shown for three independent experiments. Statistically significant differences are indicated with two stars ($p<0.0001$).

Supplementary Videos

Video S1: Visualisation of TdT::IFT81 in AnTat1.1E cells.

TdT::IFT81 is found inside the trypanosome flagellum where it travels by IFT. Live procyclic, wild-type *T. brucei* cell transfected with TdT::IFT81 observed by time-lapse epifluorescence microscopy using a DMI4000 microscope at room temperature. Frames were taken every 100 ms for 30 s by an Evolve 512 EMCCD Camera. Example of a cell with a single flagellum.

Video S2: Visualisation of TdT::IFT81 in AnTat1.1E cells.

Same as Video S1 but example of a cell with two flagella, the new one being at early phase of assembly.

Video S3: Visualisation of TdT::IFT81 in 1.1E cells.

Same as Video S1 but example of a cell with two flagella, the new one being at an intermediate phase of assembly.

Video S4: Visualisation of TdT::IFT81 in AnTat1.1E cells.

Same as Video S1 but example of a cell with two flagella, the new one being at a late phase of assembly.

Video S5: Visualisation of TdT::IFT81 in $KIN2A2B^{RNAi}$ cells.

This is an example of a non-induced cell showing robust IFT. IFT proteins are found at the base of the flagellum and as motile trains trafficking both ways in the flagellum.

Video S6: Visualisation of TdT::IFT81 in $KIN2A2B^{RNAi}$ cells.

This is an example of a cell induced for 6 days where the frequency of IFT is much reduced whereas the total amount of IFT protein at the base is significantly increased.

Table 1 IFT speed and frequency in growing and mature flagella of AnTat1E cells expressing TdT::IFT81. The number of measured trains is given in parentheses. Since retrograde trains are more difficult to detect, only non-ambiguous ones were used for analysis, hence the reduced number. There are no statistically significant differences for all parameters between uniflagellated and biflagellated cells with the exception of the speed of anterograde trains in the old flagellum of biflagellated cells compared to the new one (p=0.06).

		Uniflagellated cells	Biflagellated cells	
			New F	Old F
Speed ($\mu m.sec^{-1}$)	Anterograde	1.65 ± 0.36 (329)	1.63 ± 0.40 (396)	1.9 ± 0.53 (419)
	Retrograde	5.09 ± 0.86 (297)	5.29 ± 0.60 (284)	5.38 ± 1.0 (261)
Frequency ($trains.sec^{-1}$)	Anterograde	1.13 ± 0.21	1.00 ± 0.22	1.04 ± 0.33
	Retrograde	1.59 ± 0.28	1.78 ± 0.84	1.7 ± 0.63

Table 2. IFT anterograde speed and frequency in the *KIN2A2B*^{RNAi} cell line in various conditions

Conditions	Frequency (train.sec^{-1})	Speed (µm sec^{-1})	Trains
No tetracycline	0.63 ± 0.08	1.78 ± 0.51	159
1-day induction	0.38 ± 0.06	1.91 ± 0.64	95
4-day induction	0.28 ± 0.09	1.32 ± 0.65	62
6-day induction	0.25 ± 0.07	1.40 ± 0.59	63
De-induced (OF)	0.38 ± 0.11	-	161
De-induced (NF)	0.50 ±0.13	-	239

In the case of conventional tetracycline induction of RNAi, only cells possessing a single flagellum was used for the analysis. In the case of the de-induction experiment, only cells with two nuclei and two flagella were measured. IFT speed was not measured in these experiments. OF, old flagella; NF, new flagella.

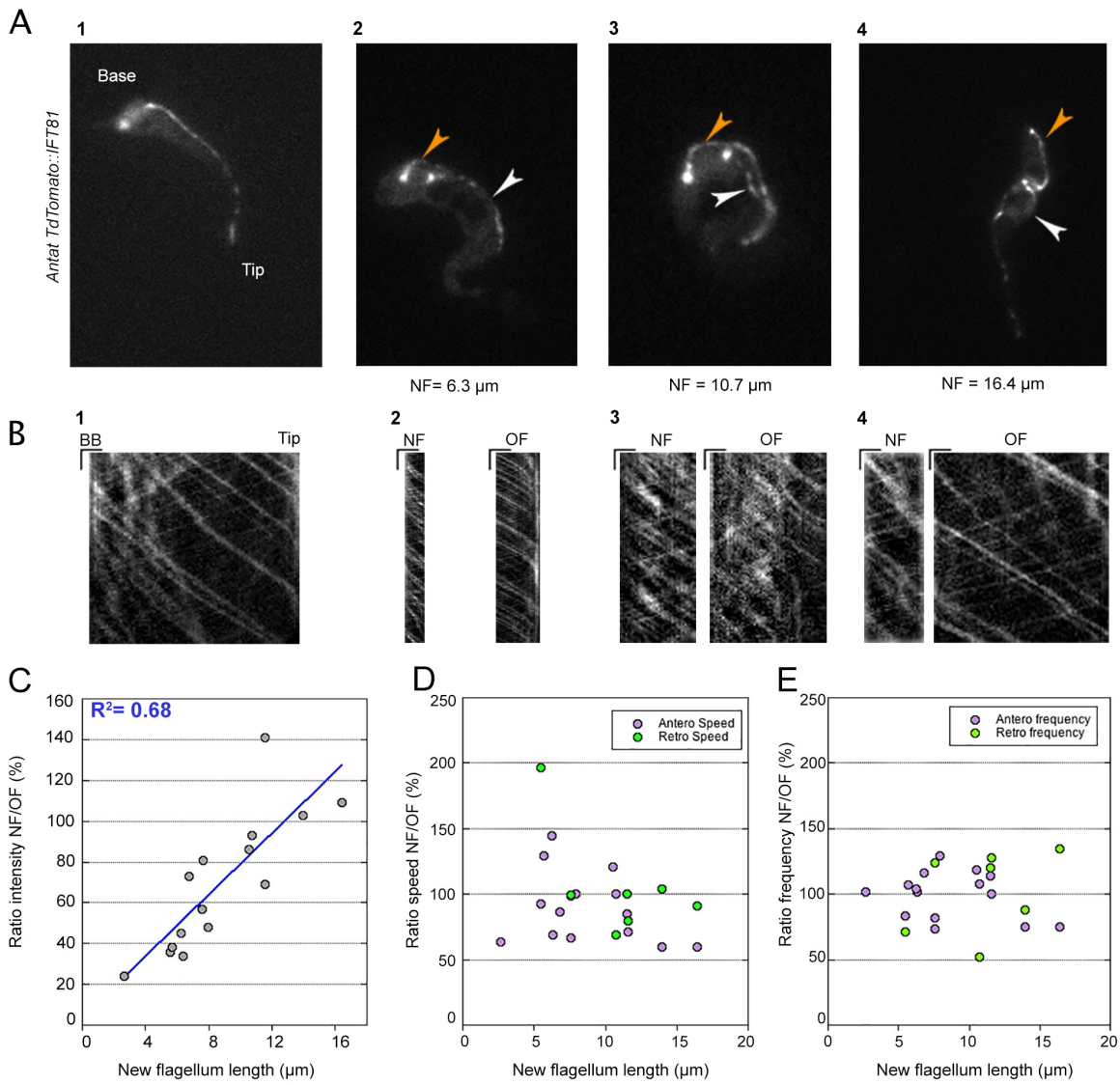
A
1
2
3
4
Base
Tip
Antat TdTomato::IFT81
NF= 6.3 µm
NF = 10.7 µm
NF = 16.4 µm
B
BB
Tip
NF
OF
C
R²= 0.68
Ratio intensity NF/OF (%)
New flagellum length (µm)
D
Antero Speed
Retro Speed
Ratio speed NF/OF (%)
New flagellum length (µm)
E
Antero frequency
Retro frequency
Ratio frequency NF/OF (%)
New flagellum length (µm)

Figure 1

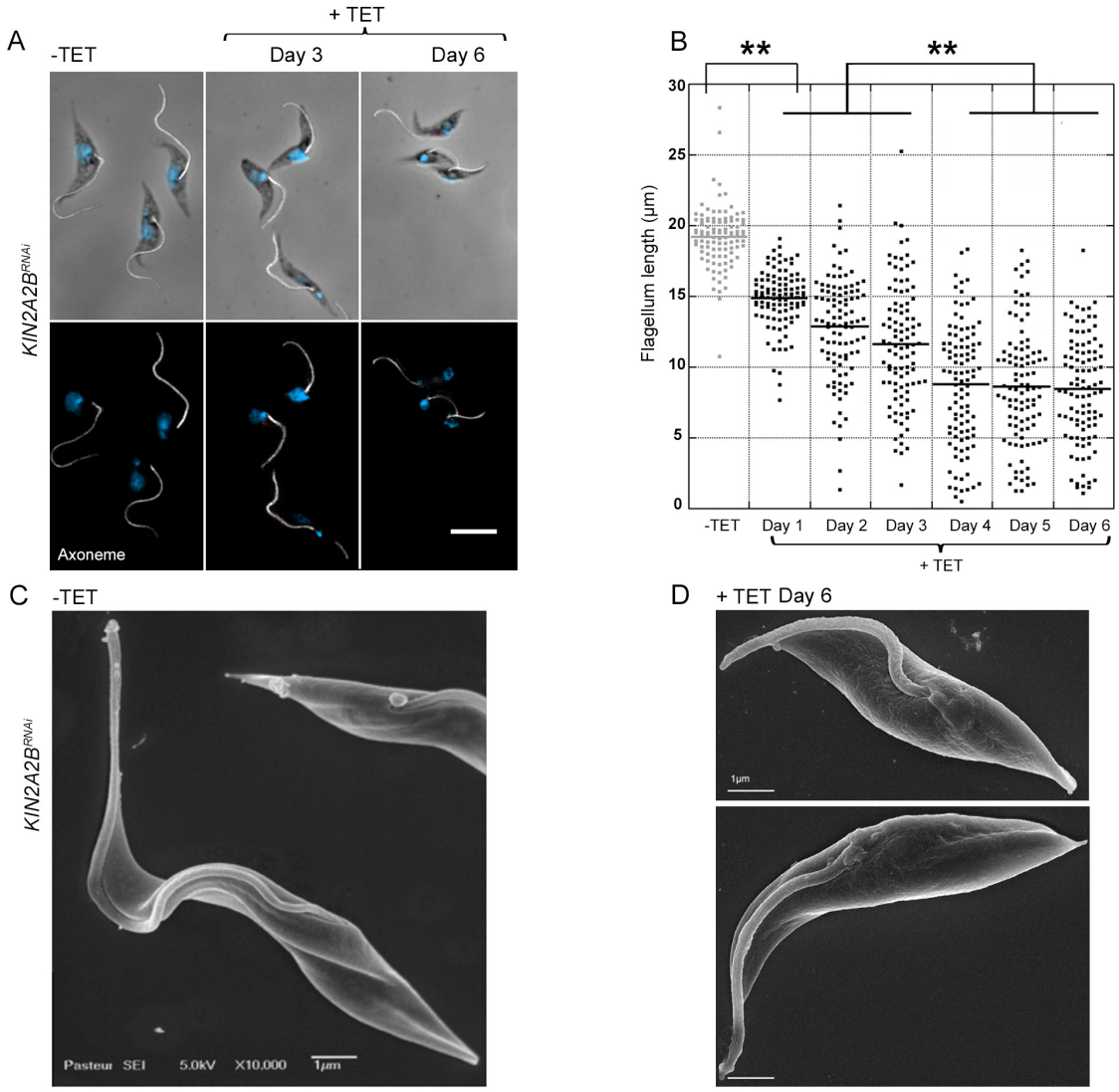
A
+ TET
-TET
Day 3
Day 6
KIN2A2B^RNAi
Axoneme
B
**
**
Flagellum length (µm)
30
25
20
15
10
5
0
-TET
Day 1
Day 2
Day 3
Day 4
Day 5
Day 6
+ TET
C
-TET
KIN2A2B^RNAi
Pasteur SEI 5.0kV X10,000 1µm
D
+ TET Day 6
1µm

Figure 2

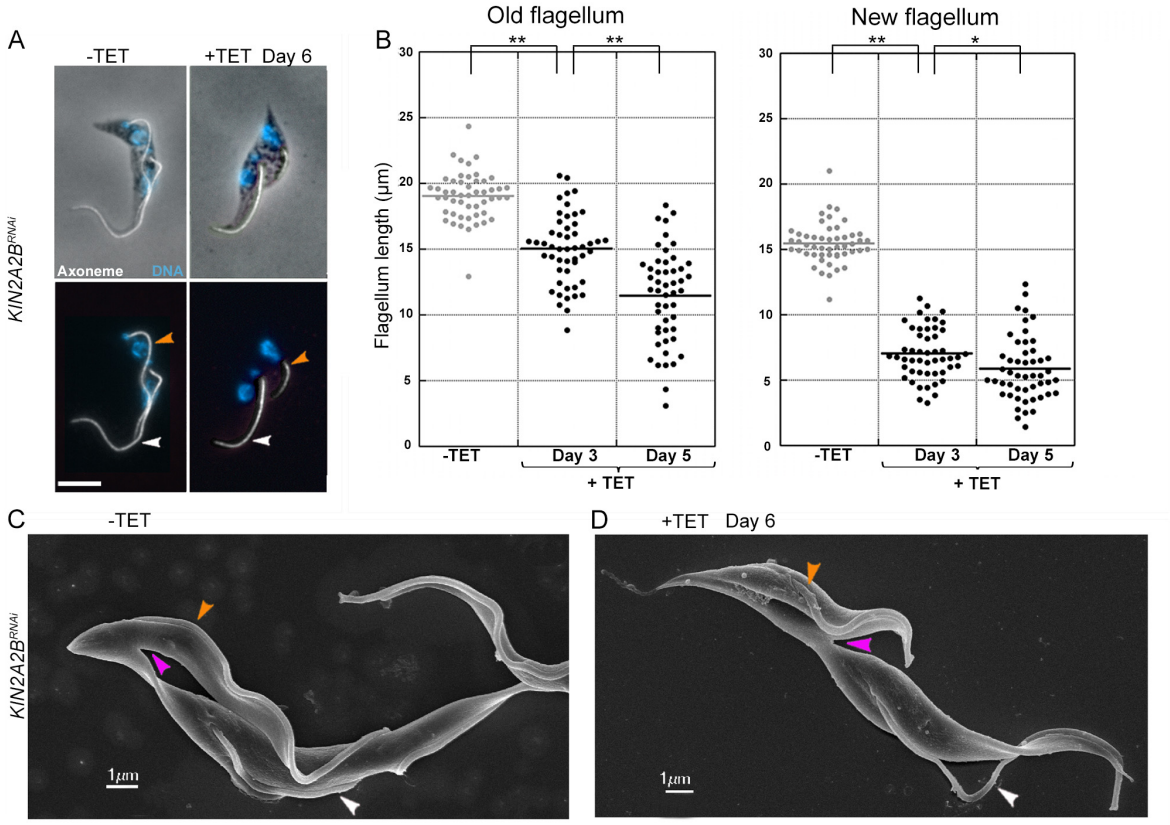
A
-TET
+TET Day 6
KIN2A2B^RNAi
Axoneme
DNA
B
Old flagellum
New flagellum
Flagellum length (µm)
**
**
**
*
-TET
Day 3
Day 5
+ TET
C
-TET
D
+TET Day 6
1µm
1µm

Figure 3

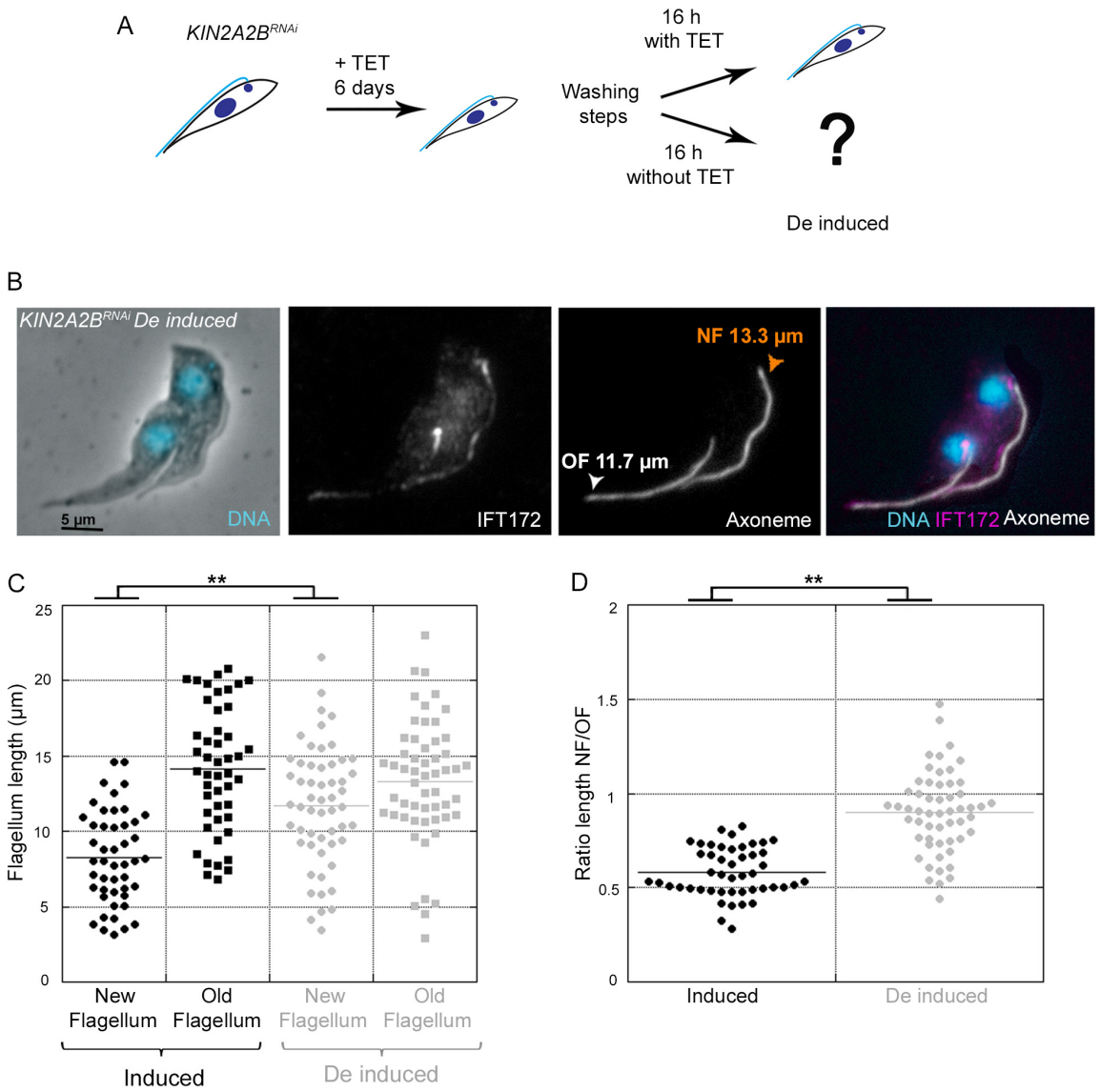
A
KIN2A2B^RNAi
+ TET
6 days
Washing
steps
16 h
with TET
16 h
without TET
?
De induced
B
KIN2A2B^RNAi De induced
5 µm
DNA
IFT172
NF 13.3 µm
OF 11.7 µm
Axoneme
DNA IFT172 Axoneme
C
**
Flagellum length (µm)
New
Flagellum
Old
Flagellum
New
Flagellum
Old
Flagellum
Induced
De induced
D
**
Ratio length NF/OF
Induced
De induced

Figure 4

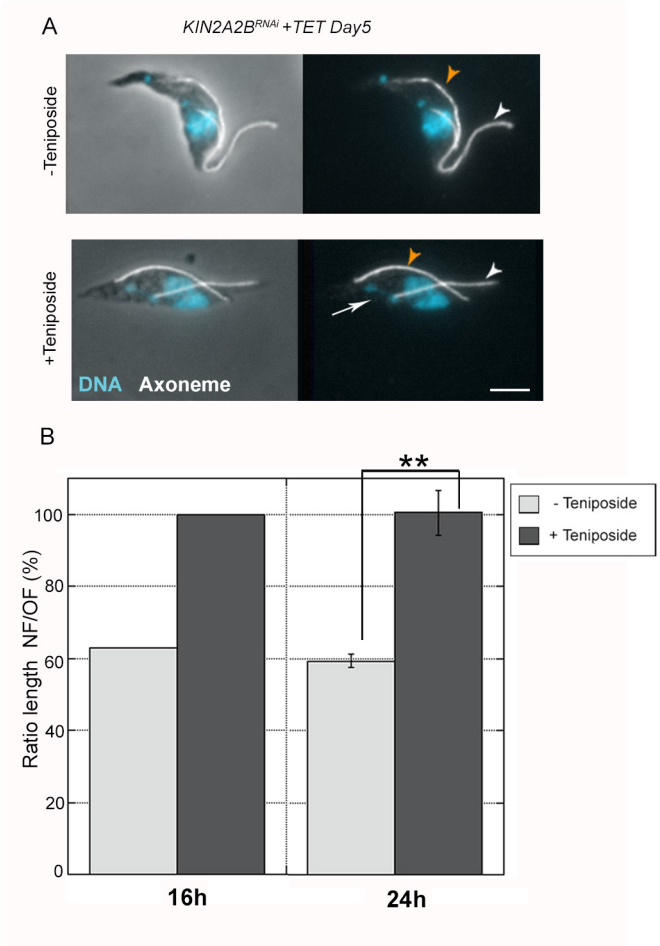
A
KIN2A2B^RNAi +TET Day5
-Teniposide
+Teniposide
DNA
Axoneme
B
**
- Teniposide
+ Teniposide
Ratio length NF/OF (%)
100
80
60
40
20
0
16h
24h

Figure 5

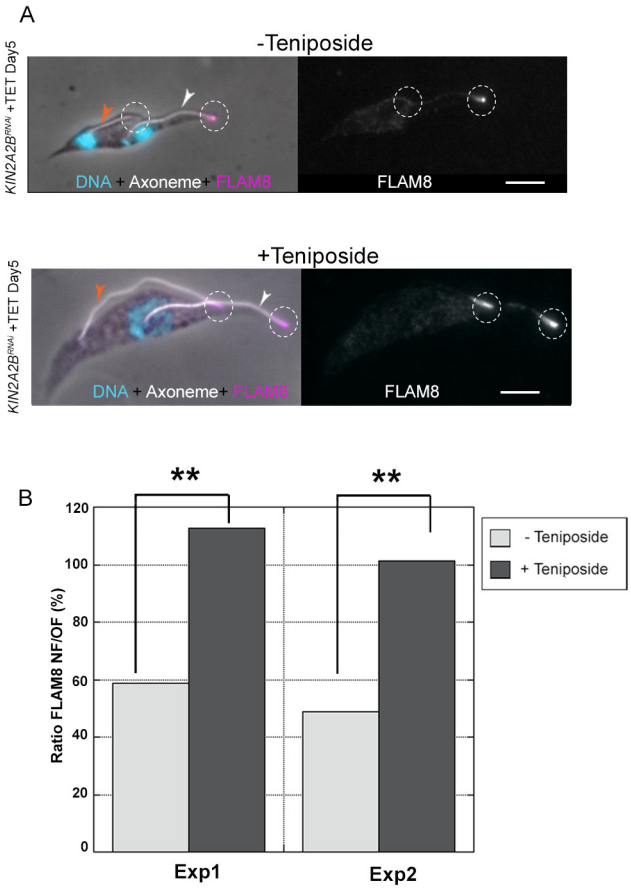
A
-Teniposide
KIN2A2B RNAi +TET Day5
DNA + Axoneme+ FLAM8
FLAM8
+Teniposide
KIN2A2B RNAi +TET Day5
DNA + Axoneme+ FLAM8
FLAM8
B
**
**
Ratio FLAM8 NF/OF (%)
120
100
80
60
40
20
0
Exp1
Exp2
- Teniposide
+ Teniposide

Figure 6

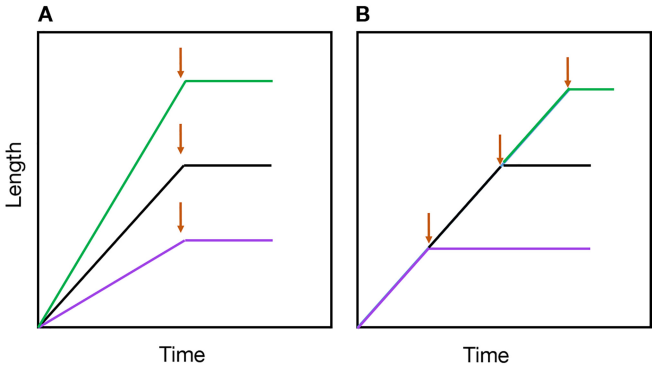

Figure 7

Figure 7

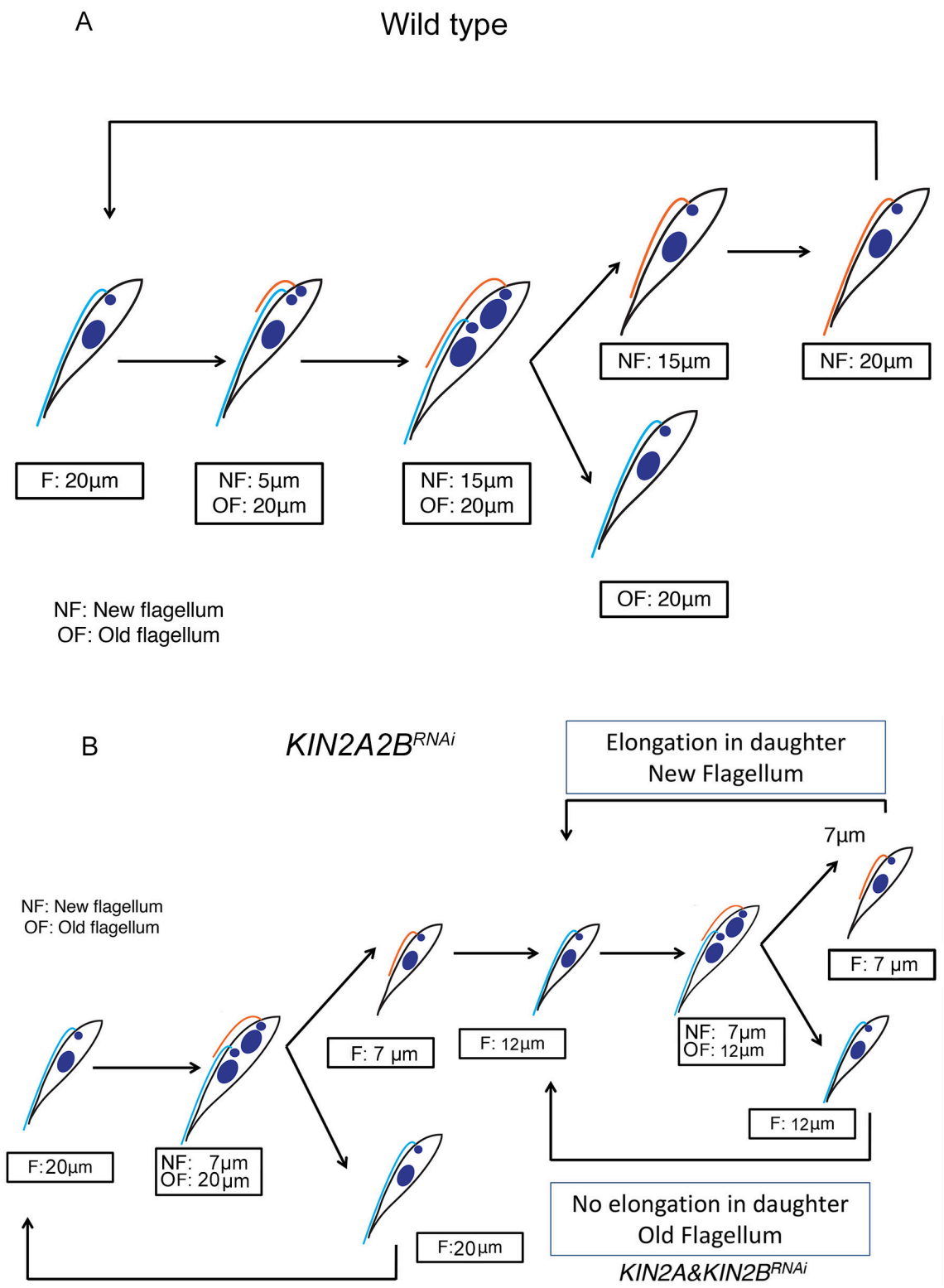
A
Wild type
F: 20µm
NF: 5µm
OF: 20µm
NF: 15µm
OF: 20µm
NF: 15µm
NF: 20µm
OF: 20µm
NF: New flagellum
OF: Old flagellum
B
KIN2A2B^RNAi
Elongation in daughter
New Flagellum
7µm
NF: New flagellum
OF: Old flagellum
F:20µm
NF: 7µm
OF: 20µm
F: 7 µm
F: 12µm
NF: 7µm
OF: 12µm
F: 7 µm
F: 12µm
F:20µm
No elongation in daughter
Old Flagellum
KIN2A&KIN2B^RNAi

Figure S1

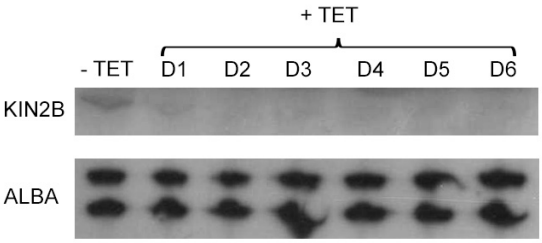

Figure S2

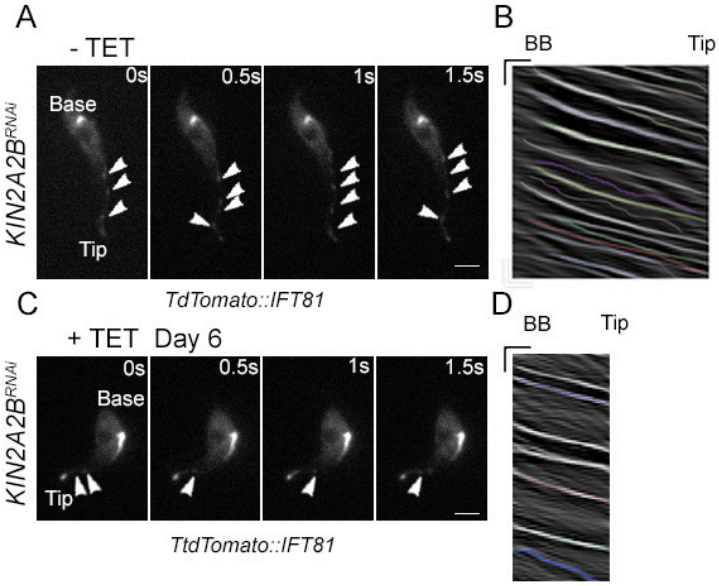

Figure S3

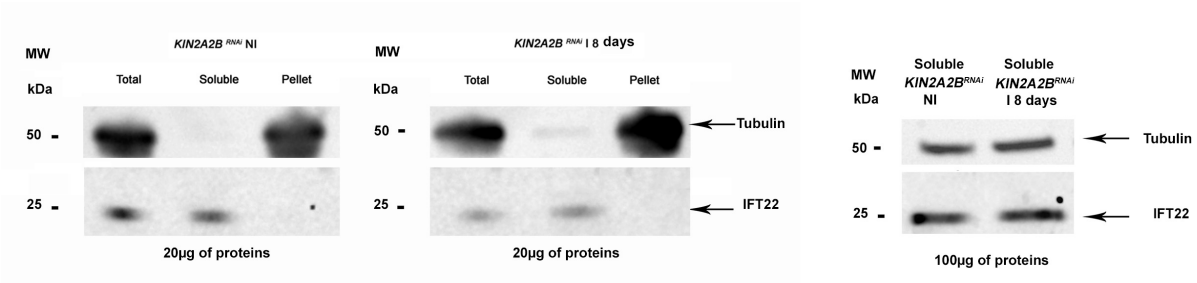

Figure S4

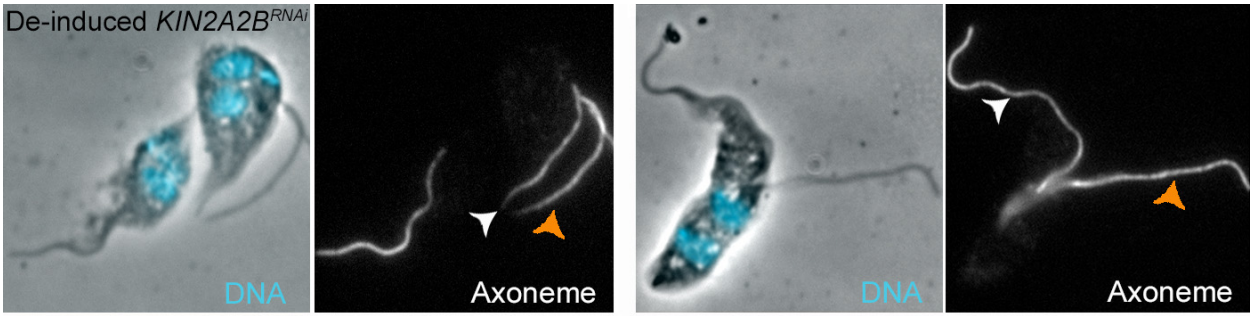

Figure S5.

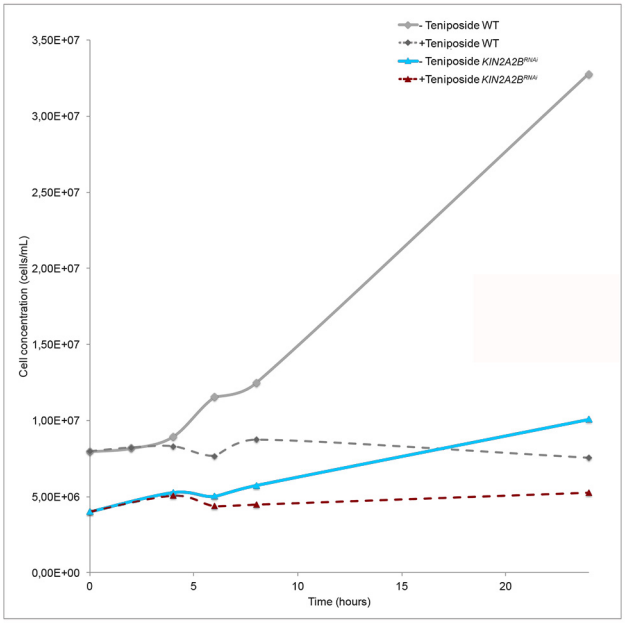
- Teniposide WT
+Teniposide WT
- Teniposide KIN2A2B^RNAi
+Teniposide KIN2A2B^RNAi
3,50E+07
3,00E+07
2,50E+07
2,00E+07
1,50E+07
1,00E+07
5,00E+06
0,00E+00
Cell concentration (cells/mL)
0
5
10
15
20
Time (hours)

Figure S6

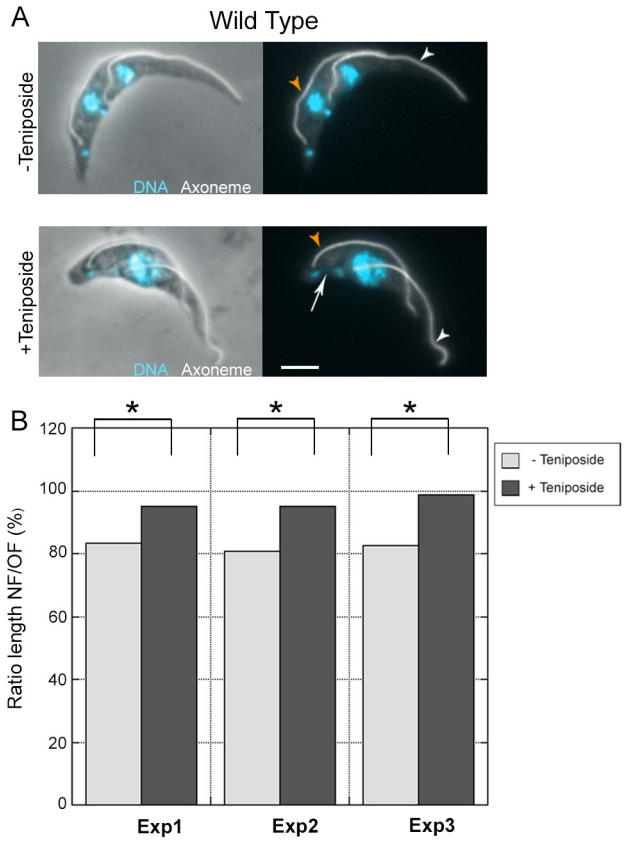
A
Wild Type
- Teniposide
+ Teniposide
DNA
Axoneme
B
Ratio length NF/OF (%)
120
100
80
60
40
20
0
*
*
*
- Teniposide
+ Teniposide
Exp1
Exp2
Exp3

Figure S7